Abstract

The MOHID 2000 system was implemented in the Tagus estuary. Interactions between hydrodynamic, cohesive-sediments and water quality were studied. The system was calibrated comparing with field data. Transport was supported by recorded hydrodynamic results considering the M2 tide constituent. This methodology allows reducing drastically the compute time. The sediments transport processes are computed using fluid velocities, shear stress and eddy diffusivities calculated by the hydrodynamic model and bottom shear stress caused by waves. The sediment transport model deeply interacts with the water quality model due to the crucial role that suspended sediments impart to the attenuation of the available light. Water quality processes were simulated with the following considerations. Autotrophic producers consume inorganic nutrients (nitrate and ammonia) and depend on both their availability and sunlight as a source of energy for photosynthesis. Primary and Secondary producer's excretions are considered, acting as source for the nitrogen cycle. Primary producers are consumed by secondary producers, which in turn are consumed by higher trophic levels. To synthesise model results an integration tool has been developed to calculate average values (in space and time) in large areas and fluxes across the borders of those areas.

Keywords: model, hydrodynamics, water quality, sediments, Tejo, MOHID 2000.

I. Introduction

Estuaries owe their high biological productivity to the established equilibrium between the biotic and physic components. The overall system can be divided in to basic subsystems, linked by the water flow, which is influenced by hydrologic cycle (river flow) and by the tidal cycle. The main subsystems are: High production low water areas, in which the production rate exceeds the respiration rate. This subsystem exports energy and nutrients to deeper waters in the estuary and to the continental shelf. The benthos subsystem in which the respiration rate exceeds the production rate, the degradation of the organic matter from the production area is accomplished, and nutrients are regenerated, recycled and stored. Finally the biological pelagic subsystem (where we include primary and secondary producer, fishes…) moving freely between the two fixed subsystems, producing, converting and transporting nutrients and energy.

Sediment transport plays an important role in this complex cycle. Firstly the crucial role that suspended sediments impart to the attenuation of the available photosynthetically useful radiant energy. Secondly, contaminants are generally transported along with the sediments upon which they are adsorbed or deposited. Finally the deposition of nutrient rich organic detritus and its subsequent biological decomposition means that estuarine sediments act as both sink and source of nutrients such phosphorus and nitrogen.

The physical behavior of sediments is related to both wave and current induced bottom stress. The waves act as a destabilization, mobilization and suspension factor for the sediments, and a minimal current may be able to carry away the already activated sediment grains. In essence, the effect of both current and waves in the sediment resuspension and transport process can be viewed as inseparable.

Objectives

Models for water quality have many purposes: aiding experimental design; linking cause and effect; running different scenarios for hypothetical situations or in a general way predicting evolution of a property field through time.

The aim of this thesis is to couple the processes described above in a overall model (Figure 1) and apply it to the Tagus estuary. With the proper calibration and parameterisation, this will allows us to gain the necessary forecast capacity and to give answers in a meaningful way to those who are responsible by the management of this ecossytem.
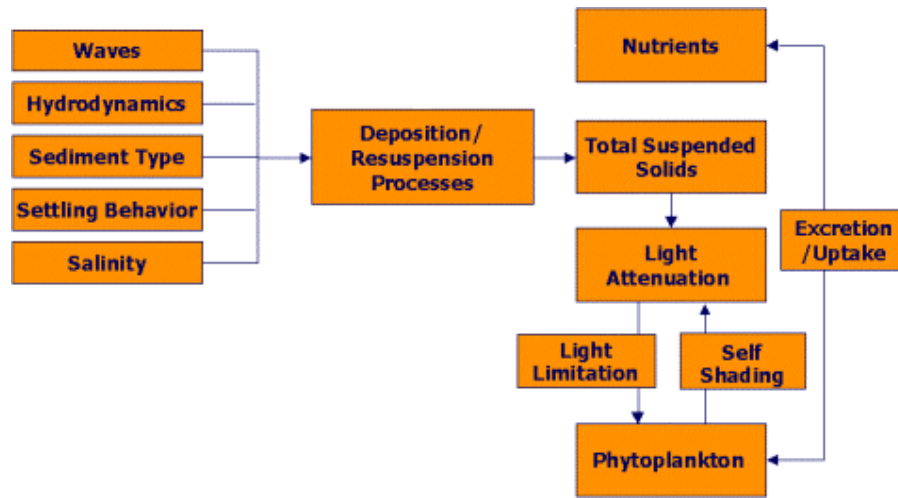
Figure 1 Schematic presentation of the processes modelled in the present thesis

Thesis Structure

The study to be done involves three major models of the MOHID 2000 modeling system: Hydrodynamics, Sediment Transport and Water Quality. In the last years there has been plenty of thesis and scientific articles describing in detail every one of these models (REF, Ref, Ref), so in the present work we will be more concerned about the linkage between them.

The thesis begins with a short description of the hydrodynamic model where we present the basic equations and explain some simplifications that where done in order to decrease the computation time. The next chapter is dedicated the sediment transport model .

II. Hydrodynamics and Transport

Hydrodynamic File

Hydrodynamic class

The hydrodynamic class solves the three-dimensional primitive equations in Cartesian coordinates for incompressible flows. Hydrostatic equilibrium is assumed as well as Boussinesq approximation. The mass and momentum evolution equations are:

$$\frac{\partial u_i}{\partial x_i} = 0 \tag{1}$$

$$\frac{\partial u_1}{\partial t} + \frac{\partial (u_j u_1)}{\partial x_j} = -fu_2 - g\frac{\rho_\eta}{\rho_0}\frac{\partial \eta}{\partial x_1} - \frac{1}{\rho_0}\frac{\partial p_s}{\partial x_1} - \frac{g}{\rho_0}\int_z^\eta \frac{\partial \rho'}{\partial x_1} dx_3 + \frac{\partial}{\partial x_j}\left(A_j\frac{\partial u_1}{\partial x_j}\right) \tag{2}$$

$$\frac{\partial u_2}{\partial t} + \frac{\partial (u_j u_2)}{\partial x_j} = fu_1 - g\frac{\rho_\eta}{\rho_0}\frac{\partial \eta}{\partial x_2} - \frac{1}{\rho_0}\frac{\partial p_s}{\partial x_2} - \frac{g}{\rho_0}\int_z^\eta \frac{\partial \rho'}{\partial x_2} dx_3 + \frac{\partial}{\partial x_j}\left(A_j\frac{\partial u_2}{\partial x_j}\right) \tag{3}$$

$$\frac{\partial p}{\partial x_3} = -\rho g \tag{4}$$

Where u_i are the velocity vector components in the Cartesian x_i directions, η is the free surface elevation, f the Coriolis parameter, A_i the turbulent viscosity and p_s is the atmospheric pressure. ρ is the density and ρ' its anomaly.

The flow field computed by the Hydrodynamic class is used to compute advection-diffusion equation (5).

$$\frac{\partial P}{\partial t} + u_i\frac{\partial P}{\partial x_i} = \frac{\partial}{\partial x_i}\left(K_i\frac{\partial P}{\partial x_i}\right) + Sources - Sinks \tag{5}$$

The density is calculated as a function of temperature and salinity by the equation of state (6):

$$\rho = \left(5890 + 38T - 0.375T^2 + 3S\right)/\left(\left(1779.5 + 11.25T - 0.0745T^2\right) - \left(3.8 + 0.01T\right)S + 0.698\left(5890 + 38T - 0.375T^2 + 3S\right)\right) \tag{6}$$

The model solves the three-dimensional primitive equations in rectangular coordinates for incompressible flows. Hydrostatic equilibrium is assumed as well as Boussinesq approximation.

The volumetric mass is calculated as a function of temperature and salinity by a constitutive law [Leendertsee and Liu, 1978]. The computed flow field transports salinity, temperature and any other tracer using an advection-diffusion equation.

The model uses a semi-implicit ADI algorithm with two time levels per iteration. Two schemes are currently implemented: the 4 equations S21 scheme [Abbott et al. 1973] and the 6 equations [Leendertse, 1967].

The free surface elevation is computed through integration of the continuity equation over the water column. Vertical fluxes are also calculated by continuity (hydrostatic approach), integrating over each cell volume. Since the grid lines are allowed to move along the vertical direction the computation of the vertical fluxes and the redefinition of the geometry are calculated in conjunction.

The model uses initial conditions of the Dirichlet type and implement five different types of boundary conditions: free surface, bottom, lateral closed boundary, lateral opened boundary and moving boundary. Moving boundaries are closed boundaries whose position varies with time. This type of situation arises in domains with inter-tidal zones, in this case the uncovered cells must be tracked and the closed boundary conditions are imposed to the surrounding covered cells.

The model solves the equations in the real domain without any space transformation. The geometry information is carried in the areas and volumes needed to calculate the fluxes. The cells can have any initial shape and suffer any time deformation allowing several vertical discretizations. This flexible architecture is equivalent to a generic vertical coordinate, the same code can be used with every coordinate and different discretizations can be used simultaneously in different regions of the domain.

In the generic coordinate approach the model must be able to solve the governing equations in a grid with any kind of geometry.

 With a finite volume method the equations are solved in the real space integrated over each cell. The cell can have any shape since in integral form only the fluxes between adjacent cells are computed. In this way a complete separation between the physical variables and the geometry is accomplished for all mesh types. In the finite volume method the geometry information is stored in the areas, volumes and faces normal directions. This information is actualized in each time step as a function of the mesh type.

All the results presented were accomplished using recorded hydrodynamic results during a semidiurnal tide cycle. A usual simulation is runned during the period of a tide cycle (12h and 25 min) and the water fluxes and elevations results are saved in a data file. Afterwards the model computes transport by reading and repeating the recorded information every semidiurnal cycle. This methodology allows us to reduce drastically the compute time (30 to 50 times faster) because the model doesn't need to compute the velocity field in every time instant. Nevertheless this is a tradeoff solution because although it allows to run the water quality model for a meaningful time scale (2, 3 years or more) in 24 to 48 hours, it despises hydrodynamic longer time scale effects like the fortnightly cycle.

III. Cohesive Sediment Modelling

Origin

The major portion of the terrigenous material that reaches the estuarine and shallow marine environments is derived from the continents through weathering processes and transport via river systems. The products of continental weathering and erosion are transported in the form of suspended particulate matter, colloidal materials, and dissolved species. The behaviour of each material is dictated by its chemical composition and physical properties, and by the chemical, physical, and biological constraints imposed upon it by the estuarine environment.

Floculation

Small-suspended particles are prevented from aggregating by electrostatic repulsion between the electrical double layers (adsorbed-ion layer and counter-ion layer). In low saline water this double layer forms easily and suspensions tend to be stable. Therefore increasing the concentration of salt in water causes a decrease in the double layer allowing particles to aggregate and settle. From fieldwork (Wollast, 1986), there is clear evidence that an intensive flocculation occurs as soon as salinity reaches about 1‰ and is complete for values higher than 2.5‰. In the Tagus estuary, these conditions are usually met downstream from Vila Franca de Xira.

The probability of particles to aggregate into flocs depends also on the probability of the particles to collide. This probability is proportional to the concentration, and also increases with the amplitude and frequency of the turbulent random movement. Aggregation is a reversible process. Flocs are fragile and, if submitted to shear, they can disaggregate. Because shear increases also with turbulence intensity the latter plays a double role in the aggregation process.

Settling Velocity

The settling flux of cohesive sediment in turbulent flows is strongly dependent on the sediment concentration; this is due to the fact that the settling velocity itself depends on the concentration. Moreover, the settling velocity of cohesive materials is a function of the suspension and not exclusively of the sediment (Mehta, 1988). This aspect can be understood if the causes for aggregation of of cohesive particles are considered.

Aggregation or flocculation occurs as a consequence of the net attractive forces between particles, brought close enough by Brownian motion, differential settling and current shear. Although the relative importance of collision frequency due to the above mechanisms depends on the particle diameter, current shear seems to be the most important factor contributing to aggregation, with the exception of slack water periods when differential settling becomes dominant (Mehta, 1988). Aggregates or flocs are formed of individual particles and can, themselves, form aggregates of higher orders. They differ from primary particles in four main aspects :

- Their size is larger than that of individual particles;
- their density is less than that of the particles due to interstitial water;
- their shape is more spherical than the plate-like shape of the primary particles, which corresponds to reduced drag;
- they are extremely weak, tending to break up.

The most significant of the above factors are the increase in diameter and the reduction of the drag and the settling velocities of the flocs are higher than those of the individual particles. To simulate the effect of flocculation a test was incorporated that sets the settling velocity to zero if salinity is lower then 3‰.

The dependence of the settling velocity on concentration neglecting the usually (but not always) secondary effects of temperature and salinity, fall within three ranges as sown in Figure 2, in which the variation of the logarithm of settling velocity with logarithm concentration is depicted schematically.
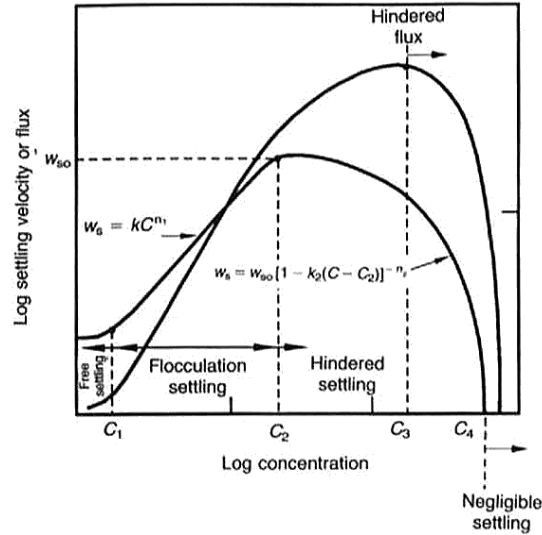
Figure 2 Variation of settling velocity and settling flux with suspension concentration (Mehta, 1994)

Free Settling

Free settling occurs for low concentrations, typically lower than 100 to 300 mg/l (Mehta, 1994). In this range the particles settle freely, without mutual interference; their settling velocity is a result of the force balance between drag and net negative buoyancy. In the viscous range ($Re_s < 1$) the drag coefficient is

$$C_D = \frac{24}{Re_s} \qquad \text{Eq. III-1}$$

(where $Re_s = W_S D / \nu$) and the settling velocity is (Vanoni, 1975)

$$W_S = \frac{D^2}{18}(\frac{\rho_s - \rho_w}{\mu})g \qquad \text{Eq. III-2}$$

where D is the grain diameter, ρ_s and ρ_w are the grain and fluid densities, g the gravitational acceleration and μ the dynamic viscosity.

Flocculation Settling

For higher suspension concentrations than the free settling limit, an increase in aggregation causes higher settling velocities, generally expressed as:

13

$$W_S = k_1 C^{n_1} \qquad \text{Eq. III-1}$$

Hindered Settling

Models representing cohesive sediment by a bulk concentration use a bulk settling velocity. If no information is available on the type of particles in the system and no evolution equation is solved for each class of flocs, then it is not possible to explicitly represent the flocculation processes in this type of correlation. The general correlation for the settling velocity in the flocculation range

$$W_S = K_1 C^m \qquad \text{for} \quad C < C_{HS}, \qquad \text{Eq. III-3}$$

and in the hindered settling range is:

$$W_S = K_1 C_{HS}{}^m \left[1.0 - K_2 \left(C - C_{HS}\right)\right]^{m_1} \quad \text{for} \quad C > C_{HS} \qquad \text{Eq. III-4}$$

where W_S (ms^{-1}) is the settling velocity, C (kgm^{-3}) is the concentration, and the subscript HS refers to the onset of the hindered settling (of about 2 to 5 kgm^{-3}). The coefficients K_1 (m^{4}kg^{-1}s^{-1}) and K_2 (m^{3}kg^{-1}) depend on the mineralogy of the mud and the exponents m and m_1 depend on particle size and shape.

Krone (1962), based on the kinetics of flocculation, proposed a theoretical value for m equal to 4/3. Mehta (1986) found, experimentally, values varying between 1 and 2. The exponent m_1 is usually taken as 4.65 for small particles and 2.32 for large particles (Dyer, 1986). To ensure that both equations are dimensionally correct, both m and m_1 should be 1.

The Transport Equation

The cohesive sediment transport is governed by a 3D advection-diffusion equation where the vertical advection includes the particle settling velocity. The equation is derived by considering a differential control volume and equating the time rate of sediment accumulation inside the volume to the net flux of sediment through its boundaries. This approach is a consequence of the assumption that, despite the continuous process os floc formation and destruction within the control volume, the overall sediment size distribution remains constant and no production or decay terms need to be added to the equation and suspended sediment can be assumed to behave conservatively. The equation is then

$$\frac{\partial C}{\partial t} = -\vec{\nabla} \cdot \vec{N}$$

Eq. III-5

where C is the suspended sediment concentration (mass of sediment / volume of suspension) and $\vec{N}$ is the net sediment flux vector. This vector can be decomposed into an advective component, a molecular diffusion component, and a settling component, since the sediment is not neutrally buoyant.

$$\vec{N}_A = \vec{v}C$$

Eq. III-6

$$\vec{N}_D = -D_m \vec{\nabla} C$$

Eq. III-7

$$\vec{N}_S = -W_S C \vec{k}$$

Eq. III-8

where $\vec{v}$ is the fluid velocity vector, D_m the Fickian molecular diffusion coefficient, W_S the terminal settling velocity of the sediment particles or flocs and $\vec{k}$ the vertical unity vector (upwards). This leads to

$$\frac{\partial C}{\partial t} = -\vec{\nabla} \cdot (\vec{v}C - D_m \vec{\nabla} C - W_S C \vec{k})$$

Eq. III-9

Decomposing the flow velocity components and concentrations into time averaged parts (over a period longer than the turbulent time scales involved), denoted by an overbar, and fluctuating components, denoted by a prime, inserting these terms into, Eq. III-9 averaging over the same time scale, the following equation is obtained :

$$\frac{\partial \overline{C}}{\partial t} + \vec{\nabla}\overline{\vec{v}}\overline{C} = D_m \nabla^2 \overline{C} + \vec{\nabla} \cdot (W_S \overline{C} \vec{k}) + \vec{\nabla} \cdot (-\overline{\vec{v}'C'})$$

Eq. III-10

which can also be written as

$$\frac{\partial \overline{C}}{\partial t} + \frac{\partial(\overline{u}\,\overline{C})}{\partial x} + \frac{\partial(\overline{v}\,\overline{C})}{\partial y} + \frac{\partial(\overline{w}\,\overline{C})}{\partial z} = D_m(\frac{\partial^2 \overline{C}}{\partial x^2} + \frac{\partial^2 \overline{C}}{\partial y^2} + \frac{\partial^2 \overline{C}}{\partial z^2}) + \frac{\partial}{\partial z}(W_S \overline{C}) - \frac{\partial}{\partial x}(\overline{u'C'}) - \frac{\partial}{\partial y}(\overline{v'C'}) - \frac{\partial}{\partial z}(\overline{w'C'})$$

Eq. III-11

The last three terms in Eq. III-11 correspond to gradients of turbulent diffusion fluxes, commonly modeled as:

$$-\frac{\partial}{\partial x}(\overline{u'C'}) = -\frac{\partial}{\partial x}(-\varepsilon_x \frac{\partial \overline{C}}{\partial x})$$ Eq. III-12

$$-\frac{\partial}{\partial y}(\overline{v'C'}) = -\frac{\partial}{\partial y}(-\varepsilon_y \frac{\partial \overline{C}}{\partial y})$$ Eq. III-13

$$-\frac{\partial}{\partial z}(\overline{w'C'}) = -\frac{\partial}{\partial z}(-\varepsilon_z \frac{\partial \overline{C}}{\partial z})$$ Eq. III-14

where ε_x, ε_y, ε_z are the turbulent mass diffusion coefficients, in the x, y, z directions, respectively. Turbulent diffusivities are, however, much larger than the molecular diffusivities and the terms corresponding to the latter phenomenon can be neglected in Eq. III-11, which becomes :

$$\frac{\partial(C)}{\partial t} + \frac{\partial(uC)}{\partial x} + \frac{\partial(vC)}{\partial y} + \frac{\partial((w+W_s)C)}{\partial z} = \frac{\partial}{\partial x}(\varepsilon_x \frac{\partial C}{\partial x}) + \frac{\partial}{\partial y}(\varepsilon_y \frac{\partial C}{\partial y}) + \frac{\partial}{\partial z}(\varepsilon_z \frac{\partial C}{\partial z})$$ Eq. III-15

The last equation is valid in the water column, and requires appropriate boundary conditions. These are (Ross, 1988):

Bed Boundary Condition

At the bed, $z = Z_b$, a bed flux term, F_b, (mass of sediment per unit bed area per unit time) must be defined, corresponding to a source or sink for the suspended sediment in conditions of erosion or deposition, respectively. Consequently, in the z direction, and at the bed:

$$N(Z_b,t) = F_b = E - D$$ Eq. III-16

where E and D are the erosion and deposition fluxes, respectively.

Free Surface Boundary Condition

At the water surface, $z = \zeta$, a no-flux condition is necessary, corresponding to a zero total flux, the diffusion flux always balancing the settling flux. Consequently:

16

$$N(\zeta,t) = W_s C \big|_\zeta + \varepsilon_z \frac{\partial C}{\partial z}\bigg|_\zeta = 0 \qquad\qquad \text{Eq. III-17}$$

Fluxes at the bed

Although there is evidence that matter is continuously deposited and removed from the bottom, most models follow Einstein (1950) and consider that the two processes cannot occur simultaneously. In such models, it is assumed that, when bottom friction is smaller than a critical value for deposition, there is addition of matter to the bottom, and, when the bottom shear is higher than a minimum value, erosion occurs. Between those values, erosion and deposition balance each other. In fact only very recently has it been possible to measure the downward and upward movement of particles at the bottom interface. In former times the best that could be achieved was to measure the net erosion or deposition as a function of the bottom shear. Both formulations can easily be included in the same model. In this work, the traditional approach was adopted because it is much easier to find data in the literature to specify the parameters.

Erosion Flux

Erosion of cohesive sediment has generally been observed to occur in one of two modes: particle-by-particle and mass erosion. The former mode corresponds to the case in which particles separate from the bed in an individual basis, as a result of hydrodynamical forces exceeding cohesive bonding, frictional and gravitational forces; in the latter case portions of the bed become unstable and large masses of sediment are resuspended. Particle by particle erosion is, however, the most common erosion mechanism in estuaries; under the action of bottom shear stresses higher than the bed shear strength, removal of particles and decrease in bed elevation (scour) will proceed until a bed layer of higher strength, equal to the applied stress, is found. This increase in bed shear strength with depth is due to changes in the floc structure after deposition, during consolidation and gelling.

Erodibility of a cohesive bed is driven by shear, but also depends on bottom cohesive nature, which in turn depends, in a poorly understood way, on clay mineralogy and on the geochemistry and microbiological processes occurring in the bottom. Some

authors argue that it should also depend on the salinity (Hayter and Metha, 1986). However, no dependency laws have yet been advanced.

Again a useful correlation must depend only on the variables calculated by the model and on parameters. The erosion algorithm used in this work is based on the classical approach of Partheniades, (1965). Erosion occurs when the ambient shear stress exceeds the threshold of erosion. The flux of eroded matter is given by:

$$\frac{dM_E}{dt} = E\left(\frac{\tau}{\tau_E} - 1\right) \qquad \text{for} \qquad \tau > \tau_E, \qquad \text{eq. III-18}$$

$$\frac{dM_E}{dt} = 0 \qquad \text{for} \qquad \tau < \tau_E, \qquad \text{eq. III-19}$$

where τ is the bed shear stress, τ_E is a critical shear stress for erosion and E is the erosion constant ($kgm^{-2}s^{-1}$).

The parameter E (eq. III-18) depends on the physico-chemical characteristics of bottom sediment. In the Western Scheldt, Mulder and Udink, (1991) used 5×10^{-5} $kgm^{-2}s^{-1}$. As a general rule, bottom-sediments are a mixture of cohesive and non-cohesive sediments; this parameter must also account for that and so a gradient must be expected in the estuary.

Critical shear stress for erosion is a function of the degree of compaction of bottom sediments measured by the dry density of the bottom sediments: ratio between the mass of sediment (after extraction of the interstitial water at 105°C) and its initial volume.

Stephens *et al.* (1992), based on the formulations proposed by Delo (1988), used:

$$\tau_E = A_1\left(\rho_d\right)^{E_1} \qquad \text{eq. III-20}$$

where ρ_d (kgm^{-3}) is dry density of bed sediments, and A_1 (m^2s^{-2}) and E_1 are coefficients depending on mud type.

This equation is dimensionally correct only for $E_1=1$. Nevertheless Stephens *et al.* (1992) calibrated their model with $A_1=0.0012$ m^2s^{-2} and $E_1=1.2$. This is a critical point

when a compaction model is used, otherwise this correlation becomes an indirect means of imposing a critical shear stress for erosion knowing the bed sediment dry density, much easier to measure. The deviation of the coefficient E_1 from unity can be seen as a measure of the error of the input data.

The deposition Flux

The deposition flux can be defined as

$$F_p = \frac{dm}{dt} = -pW_S C \qquad \text{eq. III-21}$$

where p is the probability of sediment deposition, W_S the settling velocity and C the near-bed sediment concentration. The probability of deposition, due to Krone (1962), is defined as:

$$p = (1 - \frac{\tau_b}{\tau_{cd}}) \qquad \text{eq. III-22}$$

where τ_b and τ_{cd} are the bottom shear stress and a critical shear stress for deposition, respectively. This concept reflects the fact that the deposition of flocs is controlled by near-bed turbulence or, more specifically, by the rate of shearing $\partial u/\partial z$ at $z = z_b$. For a floc to stick to the bed it must be strong enough to withstand the the near bed shear stress

The deposition algorithm, like the erosion algorithm, is based on the assumption that deposition and erosion never occur simultaneously. An algorithm was first proposed by Krone (1962) and later on modified by Odd and Owen, (1972). The algorithm is based on the assumption that a particle reaching the bottom has a probability of remaining there that varies between 0 and 1 as the bottom shear stress varies between its upper limit for deposition and zero respectively. Deposition is calculated as the product of the settling flux and the probability of a particle to remain on the bed:

$$\frac{dM_D}{dt} = (CW_S)_B(1 - \frac{\tau}{\tau_D}) \qquad \text{for} \quad \tau < \tau_D, \qquad \text{eq. III-23}$$

$$\frac{dM_D}{dt} = 0 \qquad \text{for} \quad \tau > \tau_D, \qquad \text{eq. III-24}$$

where τ_D is the critical stress for deposition and subscript B means "at the sediment-water interface". The critical shear stress for deposition, τ_D, depends mainly on the size of the flocs. Bigger flocs have higher probability of remaining on the bed than smaller flocs. Nevertheless previous work suggest that a constant value is a reasonable approximation. Based on laboratory experiments with natural mud from the Western Scheldt, Winterwerp *et al.* (1991) found $\tau_D = 0.2$ N m^{-2}. For the Gironde, LI *et al.* (1994) used values in the range 0.3-0.5 N m^{-2}.

Waves

Waves exert friction forces at the bed during propagation. The bed shear stress, which is important for wave damping and sediment entrainment, is related to the friction coefficient by:

$$\tau_w = \frac{1}{2}\rho f_w U_\delta^2$$

In which:

τ_w Instantaneous bed-shear stress [N/m^2]

f_w Friction coefficient [dimensionless]

U_δ Instantaneous fluid velocity just outside boundary layer [m/s]

ρ Fluid density [kg/m^3]

The friction factor f_w is assumed to be constant over the wave cycle and is determined from the peak values as: $f_w = 2\tau_w / (\rho U_\delta^2)$.

The time-average (over a wave cycle) bed shear stress is:

$$\hat{\tau}_w = \frac{1}{4}\rho f_w \hat{U}_\delta^2$$

In the rough turbulent regime Jonsson (1966 in van Rijn, 1989) proposed:

$$f_w = \exp\left[-6 + 5.2\left(\frac{\hat{A}_\delta}{k_s}\right)^{-0.19}\right]$$

with $f_{w,max} = 0.3$ for $\left(\dfrac{\hat{A}_\delta}{k_s}\right) \leq 1.57$

where k_s stands for bed roughness [m]

Wave parameters

Applying linear wave theory, the peak value of the orbital excursion ($\hat{A}_\delta$) and velocity ($\hat{U}_\delta$) at the edge of the wave boundary layer can be expressed as:

$$\hat{A}_\delta = \frac{H}{\sinh(kh)}$$

$$\hat{U}_\delta = \hat{A}_\delta \varpi = \frac{H\Pi}{T \sinh(kh)}$$

in which:

$\varpi = 2\Pi / T$	Angular velocity [rad/s]
$k = 2\Pi / L$	Wave number [rad/m]
H	Wave height [m]
$L = (gt^2 / 2\Pi)\tanh(kh)$	Wave length [m]
T	Wave period [s]
H	Water depth [m]

Linear wave theory is generally applied to determine the near-bed velocities. In case of symmetrical (sinusoidal) small-amplitude waves in relatively deep water this theory yields correct results. When waves are approaching shallower waters, the waves will be distorted leading to asymmetrical wave profiles and higher order wave theories are basically necessary to determine the near-bed velocities. Surprisingly, comparisons of measured velocities and computed velocities according to linear wave theory show reasonably good results in shallow water.

Bed roughness

Wave ripples are formed once the oscillatory motion is of sufficient strength to cause general movement of the surface particles. The height and length of the ripples grow until a stable ripple is obtained depending on the prevailing conditions. When fully developed riples are generally two-dimensional, regular and have a sinusoidal shape. At larger velocities the flow separated from the riples and strong eddies are generated which can sweep the particles from the troughs to crests and vice-versa.

van Rijn (1989) relates the ripple height (Δ_r) and length (λ_r) to the peak value of the orbital excursion ($\hat{A}_\delta$) and a particle mobility parameter (ψ), as follows:

$$\frac{\Delta_r}{\hat{A}_\delta}, \frac{\Delta_r}{\lambda_r} = F(\Psi)$$

in which:

$$\Psi = \left(\hat{U}_\delta\right)^2 / \left[(\rho_{rel})g d_{50}\right]$$

ρ_{rel} relative density $\left(\dfrac{\rho_{sand} - \rho_{water}}{\rho_{water}}\right)$

Symbol	Name	Value	Unit
ρ_{sand}	Sand density	2.3	
ρ_{water}	Water density	1.025	
g	Gravity	9.8	ms^{-2}
d_{50}	Particle diameter	0.002	m
d_{90}	Particle diameter	0.003	m

van Rijn (1989) proposes the following relationships for irregular waves:

$$\frac{\Delta_r}{\hat{A}_\delta} = 0.22 \qquad\qquad \text{for } \Psi \le 10$$

$$\frac{\Delta_r}{\hat{A}_\delta} = 2.8 \times 10^{-13}(250 - \Psi)^5 \qquad \text{for } 10 \le \Psi \le 250$$

$$\frac{\Delta_r}{\hat{A}_\delta} = 0 \qquad\qquad \text{for } \Psi \ge 250$$

$$\frac{\Delta_r}{\lambda_r} = 0.18 \qquad\qquad \text{for } \Psi \le 10$$

$$\frac{\Delta_r}{\lambda_r} = 2 \times 10^{-7}(250 - \Psi)^{2.5} \qquad \text{for } 10 \le \Psi \le 250$$

$$\frac{\Delta_r}{\lambda_r} = 0 \qquad\qquad \text{for } \Psi \ge 250$$

The proposed expressions for ripple steepness $\dfrac{\Delta_r}{\lambda_r}$ are valid for non-breaking wave conditions. In case of breaking wave conditions the mobility parameter (ψ) will, in general, be larger than 250 yielding sheet flow over a flat bed. In spilling breaking

waves this may be realistic. However, in plunging breaking waves the interaction of the waves with bed is so vigorously that rather irregular bed surface may be generated.

Nikuradse (1932, in van Rijn ,1989) introduced the concept of an equivalent or effective sand roughness height to simulate the roughness of arbitrary roughness elements of the boundary. In case of a movable bed consisting of sediments the effective roughness mainly consists of grain roughness generated by skin friction forces and of form roughness generated by pressure forces acting on the bed forms.

Grain roughness is dominant when the bed is plane or when the peak orbital excursion at the bed is smaller than the ripple length.

Ripples are here in defined as bed forms with length smaller than the water depth. Riples are the dominant bed forms generated by oscillatory flow. When the near-bed orbital excursion is larger than the riple length, the ripples are the dominant roughness (form roughness) elements on the bed. Assuming hydraulic rough flow and a dominant form roughness, van Rijn (1989) proposes the following values:

For grain roughness

$$k_{s,w}^{grain} = 3d_{90} \qquad\qquad \text{for } \Psi < 250$$

$$k_{s,w}^{grain} = 3(0.04\Psi - 9)d_{90} \qquad \text{for } \Psi \geq 250$$

For form roughness

$$k_{s,w}^{form} = 16\Delta_r \frac{\Delta_r}{\lambda_r} \qquad\qquad \text{for } \Psi < 250$$

$$k_{s,w}^{form} = 0 \qquad\qquad \text{for } \Psi \geq 250$$

Finally bed roughness is determined

$$k_s = \min\left[\left(k_{s,w}^{form} + k_{s,w}^{grain}\right), 0.010\right] \quad [m]$$

IV. Water Quality Modelling

Introduction

Today, efforts towards ecological modelling are being made in most countries were water quality management is a major concern. Franz *et al.*, (1991) notice that most new generation models tend to become much more biologically and chemically diversified than earlier models, as it is now largely recognised that there is no way to simulate in sufficient detail the ecosystem behaviour without an in-depth treatment of the full cycle of organic matter.

These processes are not foreign to the preoccupations caused by the eutrophication and its various manifestations. Although there is general consensus that the inputs of nutrients to the sea must be reduced there is so far no firm scientific basis to decide upon the extent of such reductions.

An appropriate way of addressing the problem of eutrophication and of testing nutrient reduction scenarios is to simulate the phenomenon with mathematical models. It is probably correct to assume that any ecological model with a sufficiently complex internal structure and the multiple relationships that are found at the lower trophic levels will come close to an answer, provided the right time scale is applied.

The model here presented is adapted from EPA, (1985) and pertain to the category of ecosystem simulations models i.e. sets of conservation equations describing as adequately as possible the working and the interrelationships of real ecosystem components. It's not correct to say that our model describes the lower trophic levels with great accuracy. In fact the microbial loop that plays a determinant role in water systems in the recycling processes of organic waste, is very simplified in our model.

Lower trophic levels appear in nearly all marine ecosystem simulation models since there is at least a compartment "phytoplankton" required to drive the organic matter cycle. Some early models applied in the North sea were one-compartment models, especially endeavouring to simulate phytoplankton growth, in relation with the physical environment and with grazing pressure (treated as a forcing variable). Both the influence of the Lotka-Volterra equations – developed in the 1920s – and that of findings in the field of plant physiology (photosynthesis-light relationship) were

discernible. It was not long before limiting nutrient and herbivorous zooplankton were incorporated as well, as state variables in simulation models. (Fransz *et al.*, 1991)

The general model

Franz *et al.* (1991) defined the general conservation equations for an idealised marine ecosystem model. Here we have adapted their definitions and establish a system that consists in five general state variables including phytoplankton, zooplankton, dissolved nutrient, organic matter in pelagic phase, organic matter in benthic phase, pelagic bacteria, benthic bacteria.

$dN/dt =$ $- f_{12}$ (uptake by phytoplankton) $- f_{15}$ (uptake by pelagic bacteria) $+ f_{51}$ (pelagic mineralization) $+ f_{61}$ (benthic mineralization) $+ f_{01}$ (excretion by zooplankton) $+$ advection and diffusion

$dP/dt =$ $+f_{12}$ (phytoplankton growth)) $- f_{23}$ (excretion of pOM) $- (f'_{23} + f'_{24})$ (natural mortality) $- f_{20}$ (grazing) $- f_{24}$ (phytoplankton sinking) $+$ advection and diffusion.

$dZ/dt =$ $+ f_{20}$ (zooplankton growth) $- f_{01}$ (excretion of nutrients) $- f_{04}$ (excretion of bOM) $- f_{03}$ (excretion of pOM)

$dpOM/dt =$ $+f_{23}$ (excretion of pOM) $+ f'_{23}$ ((1-a).natural mortality of phytoplankton) $+ f_{53}$((1-b).natural mortality of pelagic bacteria) $+ f_{03}$ ((1-c).feacal pellets and detritus from upper trophic levels) $- f_{35}$ (pOM degradation by pelagic bacteria) $+$ advection and diffusion.

$dbOM/dt =$ $+f'_{24}$ ((a).natural mortality of phytoplankton) $+ f_{24}$ (phytoplankton sinking) $+f_{54}$ ((b). natural mortality of pelagic bacteria) $+ f_{64}$ (natural mortality of benthic bacteria) $+ f_{04}$ ((c).feacal pellets and detritus from upper trophic levels) $- f_{46}$ (bOM degradation by benthic bacteria) $+$ advection and diffusion.

$dpB/dt =$ $+f_{35}$ (pOM degradation) $+ f_{15}$ (N uptake) $- f_{51}$(pelagic mineralization) $- (f_{53} + f_{54})$ (natural mortality) $+$ advection and diffusion.

$dpB/dt =$ $+f_{46}$ (bOM degradation) $- f_{61}$(benthic mineralization) $-f_{64}$ (natural mortality).

Where N   concentration of dissolved inorganic nutrient

       P   concentration of phytoplankton

       Z   concentration of zooplancton

       pOM concentration of pelagic organic matter

       bOM concentration of benthic organic matter

       pB   concentration of pelagic bacteria

       bB   concentration of benthic bacteria

       a, b, c factor comprised between 0 and 1

.

The objective is to compare recent ecological models including the MOHID water quality model and identify the common features and major differences among them. Table 1 provides a synthetic view of the equations and processes most common among ecological models and Table 2 presents the identification of the models. There are of course some limitations, the depth of this study doesn't go beyond the identification of terms. This means that, for instance, I do not wish to analyse the functional way to compute light limitation factor (in this set of models there are 5 different types), just to state that it's present in all models. More detailed information on each component will be presented only for the MOHID WQ model.

	[1]									
Nutrient, N equation										
Nitrogen	✓	✓	✓	✓	✓	✓	✓	✓	✓	✓
Phosphorous	✗	✗	✓	✗	✓	✓	✓	✗	✓	✓
Silica	✗	✗	✗	✗	✓	✗	✗	✗	✓	✗
Uptake from P	✓	✓	✓	✓	✓	✓	✓	✓	✓	✓
Uptake from pB	✗	✗	✗	✗	✗	✗	✗	✓	✓	✗
Flux from Z	✓	✗	✓	✓	✓	✗	✓	✓	✓	✓
Flux from pB or pOM	✓	✓	✓	✓	✓	✓	✓	✓	✓	✓
Flux from bB or bOM	✓	✗	✓	✗	✓	✓	✓	✓	✓	✓
Ammo./Nitr. distinction	✗	✓	✓	✓	✓	✓	✓	✓	✓	✓
Phytoplankton, P equation										
Unit	N	N	C	N	N	C	C	C	CNF	C
Sub compartments	✗	✗	✗	✗	✓	✗	✓	✗	✓	✗
Gross uptake rate u	✓	✓	✓	✓	✓	✓	✓	✓	✓	✓
Light limitation	✓	✓	✓	✓	✓	✓	✓	✓	✓	✓
Self shading	✓	✓	✓	✓	✗	✓	✓	✓	✓	✓
Nutrient limitation	✓	✓	✓	✓	✓	✓	✓	✓	✓	✓
Temperature effect	✗	✗	✓	✓	✓	✗	✓	✓	✓	✓

Respiration rate	✗	✗	✓	✓	✗	✗	✗	✓	✓	✓
Excretion rate	✗	✗	✓	✓	✓	✓	✓	✓	✓	✓
Nat mort. Rate	✓	✓	✓	✓	✓	✗	✗	✓	✓	✓
Internal N pool	✗	✗	✓	✗	✗	✗	✗	✓	✓	✗
Grazing loss	✓	✓	✓	✓	✓	✗	✓	✓	✓	✓
Sinking loss	✗	✓	✓	✓	✓	✓	✓	✓	✓	✓
Pelagic organic matter, pOM equation										
Unit	N	N	C	N	NFS	NF	NF	N/C	CNF	NF
Flux from P	✓	✓	✓	✓	✓	✓	✓	✓	✓	✓
Flux from Z	✓	✓	✓	✓	✓	✗	✓	✓	✓	✓
Flux from pB	✓	✗	✗	✗	✗	✗	✗	✓	✓	✗
Mineralization	✓	✓	✓	✓	✓	✓	✓	✓	✓	✓
Part./Diss. distinction	✗	✗	✓	✓	✓	✓	✓	✓	✓	✓
Benthic organic matter, bOM equation										
Unit	N	✗	C	N	NFS	NF	NF	N/C	CNF	✗
Flux from P	✗	✗	✓	✓	✓	✓	✓	✓	✓	✗
Flux from Z	✗	✗	✗	✓	✓	✗	✓	✓	✓	✗
Flux from pOM	✓	✗	✓	✓	✓	✓	✓	✓	✓	✗
Flux from pB	✗	✗	✗	✗	✗	✗	✗	✓	✓	✗
Flux from bB	✗	✗	✗	✗	✗	✗	✗	✗	✓	✗
Mineralization	✓	✗	✓	✓	✓	✓	✓	✓		✗
Pelagic bacteria, pB equation										
Unit	N	✗	✗	✗	✗	✗	✗	N/C	CNF	
N uptake	✗	✗	✗	✗	✗	✗	✗	✓	✓	✗
pOM uptake	✓	✗	✗	✗	✗	✗	✗	✓	✓	✗
excretion	✓	✗	✗	✗	✗	✗	✗	✓	✓	✗
respiration	✗	✗	✗	✗	✗	✗	✗	✓	✓	✗
nat. mortal.	✓	✗	✗	✗	✗	✗	✗	✓	✓	✗
Benthic bacteria, bB equation										
Unit	✗	✗	✗	✗	✗	✗	✗	✗	CNF	✗
Zooplankton, Z equation										
Unit	N	N	C	N	N	✗	C	C	CNF	C
Phyto uptake	✓	✓	✓	✓	✓	✗	✓	✓	✓	✓
Excretion	✓	✓	✓	✓	✓	✗	✓	✓	✓	✓
Respiration	✗	✗	✓	✗	✗	✗	✓	✓	✓	✓
Nat. mortal.	✓	✓	✓	✓	✓	✗	✓	✓	✓	✓
Predation loss	✗	✗	✓	✗	✗	✗	✗	✓	✓	✓

Table 1 – Ecological models components identification

The phytoplankton equation is central in all models, primary production process, powered by light energy, is the necessary engine for all transfers of mass between biological compartments. Zooplankton that on early days was not explicitly modelled

it's now considered an important state variable. Depending on the models, dead organic matter will appear in the pelagic phase under the form of dissolved organic matter, suspended detritus or several pools of organic matter from highly refractory to highly labile. In some models bacteria that undertake the degradation process are explicitly modelled, but in most case there is a major short cut, since pelagic bacteria appear only implicitly in the decay rate that is incorporated in the equations for organic matter compartments. Where bottom sediment or deep layer mineralization are concerned, the relevant processes are generally simulated by benthic organic matter degradation rates that influence nutrient and organic matter concentration in the pelagic phase.

The MOHID WQ model has its major drawback on this last subject by not simulating benthic degradation. Thus we consider that most mineralization is accomplished in the water column. It is clear that the ERSEM model is by far the most complete model of all, in fact this table is very restrict and doesn't allows to present all the it's features.

No	Article
[1]	Arhonditsis et al. (2000)
[2]	Napolitano et al. (2000)
[3]	Nakata et al. (2000)
[4]	Kawamiya et al. (2000)
[5]	Guillaud et al. (2000)
[6]	Humborg et al. (2000)
[7]	Neumann (2000)
[8]	Tett and Wilson (2000) - ML model
[9]	Baretta et al. (1995) - ERSEM model
[10]	MOHID Model – Miranda (1996)

Table 2 List of models

Forcing functions and limitations

Physical forcing

The physical world enters plankton models in various way, providing the energy supply for driving the system as kinetic energy, as heat energy and as radiative energy: the environmental conditions act as transport agents by water movements, given by advection and turbulent difusion, and they determine as well the rates of biological and chemical processes.

The change of the concentration of a property (state variable) in time is described by an equation of the type:

$$\frac{dC}{dt} = \text{Turbulent difusion terms} + \text{source terms} - \text{sinks terms}$$

The term on the left hand side is called the total derivative of the state variable C; it consists of the local change and the changes due to motions of the water, passing a certain concentration C by the point of observation:

$$\frac{dC}{dt} = \frac{\partial C}{\partial t} + u\frac{\partial C}{\partial x} + v\frac{\partial C}{\partial y} + w\frac{\partial C}{\partial z}$$

Where u, v, w denote the three components of the velocity of the water, are solved by the hydrodynamic model. The turbulent diffusion terms can be parameterised according to several models and they are also solved by the hydrodynamic model. The source and sink terms are governed by chemical, biological or sedimentological processes specific to the individual property.

Growth Limitation

Many of the equations described in the next sections are written as dependent on a regulating factor, which contains the functional response of the organism to some environmental parameters such as light, nutrients, or temperature. Advection and diffusion processes as described above are the physical transport engine that will affect this environmental parameters and consequently production. As a general rule, their influence to plankton growth is translated by limitation factors, which are discussed in the next section.

When growth is a function of many resources, there is a large range of functional forms that might express the joint dependence. To control the various possibilities, it is common to think of separate resources as limiting factors reducing some theoretical maximum growth rate - factors that can be determined separately and the combined by s small number of ways.

Each growth limitation factor can range from a value of 0 to 1. A value of 1 means the factor does not limit growth (i.e. is at optimum intensity, nutrients are available in excess, etc) and a value of 0 means the factor is so severely limiting that growth is inhibit entirely.

Four major approaches have been used to combine the limiting factors:

- A multiplicative formulation in which all factors are multiplied together. This approach assumes that several nutrients in short supply will more severely limit growth than a single nutrient in short supply. The major criticism of this approach is that the computed growth rates may be excessively low when several nutrients are limiting. Also, the severity of the reduction increases with the number of limiting nutrients considered in the model, making comparison between models difficult.

- A minimum formulation in which the most severely limiting factor alone is assumed to limit growth. This formulation is based on "Liebig's law of the minimum" which states that the factor in shortest supply will control the growth of algae. The minimum formulation is often used only for nutrient limitation, with a multiplicative formulation for the light limitation factor.

- A harmonic mean formulation that combines the reciprocal of each limiting factor in the following manner:

$$f(Light, Nutrient_1, Nutrient_2, ..., Nutrient_n) = \frac{n}{\dfrac{1}{f(Light)} + \dfrac{1}{f(Nutrient_1)} + ... + \dfrac{1}{f(Nutrient_n)}}$$

where n = number of limiting factors

This formulation is based on an electronic analogy of several resistors in series. The rationale for this formulation is that it includes some interactions between multiple limiting nutrients, but is not as severely limiting as the multiplicative formulation. Under a wide range of conditions, the harmonic mean formulation and minimum formulation produce similar growth response curves (Swartzman and Bentley, 1979 in EPA, 1985).

- An arithmetic mean formulation that uses the average of each limiting factor. The rationale for this formulation is the same as for the harmonic mean formulation. However, this formulation is rarely used since it does not restrict growth enough. For example, the arithmetic mean formulation allows growth even if a critical nutrient such nitrogen is totally absent, as long other nutrients are available.

Nutrients

The present model considers nitrogen to be the only nutrient that limits phytoplankton growth. Moreover, nitrate and ammonia are considered in the same pool. But difficulties

could be encountered to subtract phytoplankton uptake from the ammonia and nitrate pool and this problem is solved by introduction of the ammonia preference factor (β_{NH4}). The nutrient limitation is expressed in a Michaelis-Menten form, with half saturation constant (K_N).

$$\Psi(N)_{Phy} = \frac{NH_4 + NO_3}{K_N + NH_4 + NO_3}$$

With: $\Psi(N)_{Phy}$: nutrient limitation, NH_4 and NO_3: ammonia and nitrate concentrations (mg N.L^{-1}) and Kn: half-saturation constant for nitrogen limitation (mg N.L^{-1}).

Temperature

The concept of THORNTON and LESSEN, (1978) is adopted to represent temperature limitation factor ($\Psi(T)$) on autotrophs and heterotrophs organisms:

$$\Psi(T) = K_A(T) \cdot K_B(T)$$

$$K_A(T) = \frac{K_1 . e^{\gamma_1.(T-T\min)}}{1 + K_1.\left(e^{\gamma_1.(T-T\min)} - 1\right)} \qquad \text{with} \qquad \gamma_1 = \frac{Ln\dfrac{K_2(1-K_1)}{K_1(1-K_2)}}{Topt_{\min} - T\min}$$

$$K_B(T) = \frac{K_4 . e^{\gamma_2.(T\max-T)}}{1 + K_4.\left(e^{\gamma_2.(T\max-T)} - 1\right)} \qquad \text{with} \qquad \gamma_2 = \frac{Ln\dfrac{K_3(1-K_4)}{K_4(1-K_3)}}{T\max - Topt_{\max}}$$

$Topt_{\min}$ (°C) and $Topt_{\max}$ (°C) represent the temperature interval for an optimal process, and Tmax (°C) and Tmin (°C) the maximum and minimum tolerable temperature where processes are completely inhibited. Remaining constants (K_1, K_2, K_3 and K4) control the shape of the response curve of temperature effect; these values are assumed equal for all organisms in this model. Figure 3 shows temperature limitation factor variation with increasing temperature for zooplankton and phytoplankton growth.
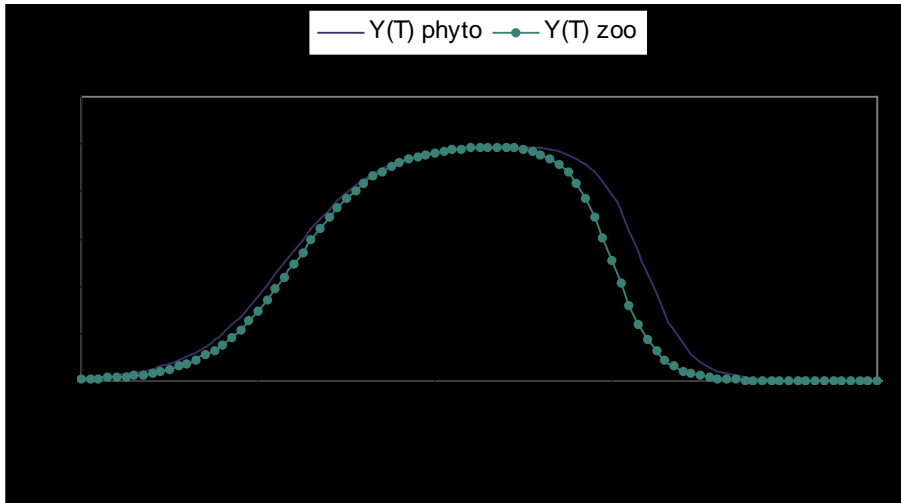
Figure 3 – Temperature limitation, $\Psi(T)$, with $K1=0.05$, $K2=0.99$, $K3=0.98$, $k4=0.02$, for phytoplankton $Topt_{min}=25$, $Topt_{max}=26.5$, $T_{min}=4$, $T_{max}=37$ ($T\ ^oC$) and for zooplankton $Topt_{min}=24.8$, $Topt_{max}=25.1$, $T_{min}=5$, $T_{max}=35$ ($T\ ^oC$)

Light

Photosynthesis is possible only when light reaching the algae cell is above certain intensity. This means that phytoplankton is limited to the uppermost layers of the water column where light intensity is sufficient for photosynthesis to occur. The depth to which light will penetrate in water, and hence the depth at which production can occur, is dependent on a number of factors; these include absorption of light by water, the wavelength of light, transparency of water, reflection from the surface of the water, reflection from suspended particles, latitude, and season of the year.

First, the simulation of solar radiation, which depends on factors such as clouds and dust in the atmosphere and the solar elevation. When light strikes the surface of water, a certain amount of light is reflected back; the amount depends on the angle at which the light strikes the surface of water. If the angle from the horizontal is low, a large amount will be reflected. Conversely, the nearer the angle is to 90º (that is perpendicular to the horizontal surface of the water), the greater will be the penetration and the lesser will be the reflection (Nybakken 1993). The angle at which the light strikes the surface of the water is directly related to the maximum height of the sun above the horizon.

Second the extinction of light in water. The extinction of light in the marine environment is one of the important water quality variables often addressed by aquatic scientists and oceanographers. The characteristics of the underwater light field itself is a

classical subject of oceanographic optics.(Rivera, 1997). The available light is one of the primary limiting variables in the growth of submerged flora, besides nutrients and temperature. Light availability is of major importance not only in determining how much plant growth will be but also which kind of species will predominate and which kind will evolve.(Rivera, 1997). Vertical light attenuation and it's spectral distribution are related to the absorption by the water itself and the following additional components of the water column: photosynthetic organisms, suspended particles and soluble compounds. Modeling light attenuation is the basis to predict the intensity and spectral composition of available light for phototropic populations (Vila *et al,* 1996).

Third, phytoplankton reaction to light. The rate of the light reaction of photosynthesis is strictly dependent on light intensity. Increases in light intensity lead to greater photosynthetic rates until some maximum is reached. At this point the producers cannot use any more light, the enzymes involved in photosynthesis cannot act fast enough to process light quanta any faster, so rate of photosynthesis reaches an asymptote. Increasingly higher light intensities usually inhibits photosynthesis (Valiela, 1995).

Solar radiation

Solar radiation is an important ecological parameter, and is often the key driving force in ecological processes (Brock, 1981). The solar radiation flux of short wavelength is compute by:

$$Q = Q_0 A_t (1 - 0.65 C_n^2)(1 - R_s)$$

Where Q_0 is the solar radiation flux on top atmosphere (Wm^2), C_n stands for cloud cover percentage and R_s stands for albedo (0.055)

The solar radiation flux on top atmosphere can be expressed as:

$$Q_0 = \frac{I_0}{r^2} \operatorname{sen} z$$

Where I_0 stands for the solar constant which is the energy received per unit time, at Earth's mean distance from the Sun, outside the atmosphere, a standard value, used is 1353 Wm^{-2} (Brock, 1981), r stands for the radious vector and z stands for the solar high.

Radius vector, r

During its revolution around the Sun, the Earth's distance varies with time of year by 3.0%, duo to the Earth's eccentric orbit. This eccentricity influences in a minor way the amount of olar radiation impinging on the Earth's surface. The radius vector of Earth's surface. The radius vector of Earth, r, expresses this ellipticity and can be calculated approximately from the following equation (Nicholls and Child, 1979 in Brock, 1981):

$$r = 1.0 + 0.017 \cos\left[2\pi \frac{(186-d)}{365}\right] \text{ [rad]}$$

where d stands for Julian Day.

Solar High

Solar radiation at any location on Earth is influenced by the motions which the Earth makes in relation to the Sun. The Earth is tilted 23.45 ° from the plane of the Earth's orbit. The declination of Earth is the angular distance at solar noon between the Sun and the Equator, north-positive. Declination depends only on the day of the year, and will be opposite in the Southern Hemisphere. The declination is obtained precisely from ephemeris tables, but can be calculated close enough for all practical purposes from the equation given by Cooper (1969 in Brock, 1981):

D1(declination) = 23.45 sin [2π(284 + N)/365]

where N is the Julian Day.
The other major motion is the daily rotation of the Earth around itself. The Earth moves 15° per hour and the sunset (or sunrise) hour –angle, W1, is the angle between the

setting Sun and the south point. The value W1 can be calculated if the latitude (L) and declination are known:

$$W1 = \arccos(-\tan(L)\tan(D1))$$

In this equation, if L and D1 are in degrees then W1 will be given in degrees. From W1, the daylength in hours, L1 ,can be calculated from the equations:

Sunrise $\quad = 12 - \frac{1}{2}L1$

Sunset $= 12 + \frac{1}{2}L1$

The hour-angle at any given time can be calculated from one of the following equations:

$$W2 = (T-12)15$$

$$W2 = 0.25 \text{ (minutes)}$$

Where T is the time (h) from midnight and minutes is the number of minutes from solar noon.

The Zenith angle or angular elevation of the Sun above the horizon, Z, can be calculated if the declination, D1, the latitude, L1, and the hour-angle, W2, are known:

$$\cos(Z) = \sin(D1)\sin(L) + \cos(D1)\cos(L)\cos(W2)$$

As a consequence of attenuation, radiation has two distinct directional properties when it reach the ground.

Direct Radiation

Direct radiation arrives from the direction of the solar disc and includes a small component scattered directly forward. The term diffuse describes all other scattered radiation received from the blue sky and from clouds, either by reflection or by transmission. Direct radiation at the ground, measured at right angles to the beam, rarely exceeds 75% of the Solar Constant, i.e. about 1030Wm^{-2}. The minimum loss of 25% is

attributable to molecular scattering and to absorption in almost equal proportions. (Monteith and Unsworth, 1990)

Diffuse radiation

Beneath a clean, cloudless atmosphere, the absolute amount of diffuse radiation increases to a maximum somewhat less then 200 Wm^2 when the zenith angle of the sun (Z) is less then 50º and the ratio of diffuse (Q_{dif}) to total radiation (Q_0) falls between 0.1 and 0.15. With increasing cloud amount also, Q_{dif}/ Q_0 increases and reaches unity when the sun is obscured by dense cloud: but the absolute level of Q_d is maximal when cloud cover is about 50%.

The coefficient for atmospheric transmission is computed by the method followed by Rosati and Miyakoda (1988 in Portela, 1996) :

$$A_t = A_{dir} + A_{dif}$$

where A_{dir} is the direct fraction and A_{dif} is the diffuse fraction of solar radition on top atmosphere that reaches the surface under a clear sky.

Direct fraction (A_{dir})

$$A_{dir} = \tau^m$$

Where $\tau = 0.74$ is atmospheric transmission coefficient for direct radiation and m the sectional mass, compute by the following expression:

$$m = 1/ sen (Z) , z = \text{zenith angle (rad)}$$

Diffuse fraction (A_{dif})

$$A_{dif =} \frac{1 - A_a - A_{dir}}{2}$$

Where $A_0 = 0.09$ is the absorption coefficient due to water vapour and ozone.

Light extinction in water

Kirk (1980) defines the inherent optical properties as the absorption, scattering and beam attenuation coefficients of a medium. The absorption coefficient is defined as the fraction absorbed per unit of path length from a parallel beam of monochromatic light directed normal to an infinitesimally thin layer of medium. Similarly, the scattering coefficient is defined as the fraction scattered of the incident parallel beam divided by the path length. The beam attenuation coefficient is defined as the sum of the absorption and scattering coefficients.

By definition, the incident light field or downward irradiance in a water column refers to the instantaneous value of the downwelling radiant flux in a horizontal unit area.

Kirk (1980) differentiates between downward and upward irradiance, the first being that due to downwelling stream of light and the second duo to the upwelling stream of light. In light extinction studies, the desirable quantity is the downwelling PAR which is referred to as the downward irradiance covering the 400 – 700 nm range of the wave spectrum.. The downwelling PAR is attenuated due to both scattering and absorption processes by the optically active components in the water column.

The major light absorbing and scattering components in the water column include dissolved organic substances, dead and living plankton material, suspended inanimate particles, and water itself. These components differ in the way they absorb and scatter downward irradiance across the photosynthetic wave band.

Generally, the strong absorption in inland and estuarine waters is attributed to organic substances, gilvin and/or phytoplankton. On the other hand, scattering, as pointed by Kirk (1980), does not itself "remove" light since a scattered photon is still available for photosynthesis. However, by making the photons follow a zig-zag path, the probability of being absorbed by the absorbing components in the aquatic medium is increased. Hence, with the scattering contribution of suspended particles for example, the vertical attenuation is intensified through this mechanism.

A common method often employed in modelling the extinction of downward irradiance is to consider the influence of the major optically active components separately giving partial extinction coefficients for each component. The sum of all the

partial extinction coefficients gives the average extinction coefficient of the water column (Rivera, 1997).

Light extinction in natural waters is affected by four primary groups of substances whose composition and concentration differ in each water body giving different values of the extinction coefficient. Further more, the extinction coefficient may change with time due to the varying composition and concentrations of the primary factors. These factors, which are referred to as optically active components of the water column, include inanimate suspended solids, dead or living phytoplankton (algae), gilvin and water itself (Rivera, 1997). Parson *et al.* (1984) uses this concept when defining the extinction coefficient in the water column (k) as follows:

$$k = k_w + k_p + k_d + k_s$$

where k_w, k_p, k_d, and k_s represent diffusion and scattering of light energy due to water (w), phytoplankton (p), suspended particles other than phytoplankton (d), and dissolved matter, respectively. The suspended particles include many different forms such as clay particles, organic detritus, and organisms varying in size. Each of these extinction coefficients are highly dependent on wavelength, however acording to Parson *et al.* (1984), for the purpose of most biological events, the average extinction coefficient in the wavelength of PAR rather than the value at particular wavelengths is probably the most practical.

The partial extinction coefficients can be determined from the specific extinction coefficient and the concentration of the optically active components of the water column by the relation:

$$k_n = \kappa_n c_n$$

where k_n is the extinction coefficient of a particular component n, κ_n the specific extinction of that component and c_n the observed concentration.

The majority of the water quality models revised (e.g. Vila e Garcia-Gil, 1996 Arhonditsis *et al.* 2000, Napolitano *et al.*, 2000 Nakata *et al.*, 2000, Kawamiya *et al.*, 2000, Humborg *et al.*, 2000, Neuman, 2000, Tett and Wilson, 2000) compute the extinction coefficient considering only phytoplankton self-shading effect. The general

form of the established relation is usually like the next equation, with different set of parameters determined according to local measurements.

$$k = k_w + \kappa_{phy} c_{phy}$$

Cole and Buchak (1995) and Somlyódy, and Koncsos, (1991) are some examples were the extinction coefficient is computed considering not only the phytoplankton concentration but also sediment concentration.

Each of these specific extinction values can represent a problem of there one in terms of modelling. A usual solution is to develop a relationship based in local measurements that allow us to determine the overall extinction coefficient. This kind of relationship can be dependent on one of the factors already described (usually phytoplankton) but does not specifically distinguish between the chosen factor and other materials. Parson *et al.*, (1984) presents a equation of this kind derived from field observations carried out in the western North Atlantic, which is used by several authors (Yanagi *et al.,* 1997; Miranda 1997). This equation relates the average extinction coefficient (k) to the chlorophyll a concentration (C) for natural phytoplankton community as follows:

$$k = 0.04 + 0.0088C + 0.054C^{2/3}$$

The coefficients to compute the extinction parameter are determined by the local light conditions of the study area. Portela (1996) following the observations made by Martins e Duffner, (1982) on the Tagus estuary obtained an average value for the extinction coefficient of 4.5 m⁻1 and a median value of 3.4 m^{-1}. Portela (1996) applied a linear regression model to the observed values of extinction coefficient and the concentration of suspended sediments measured in the Tagus estuary in 1980 (Martins e Duffner, 1982). As expected, a close relation between the two variables is observed. The final regression equation is:

$$k = 1.24 + 0.036C_{ss}$$

In the present model we wish to include the effect on light attenuation due to phytoplankton and to sediment concentration. So we have taken the slope value determined by Portela (1996) and joined to the equation from Parson *et al.*, (1984) to give:

$$k = 0.04 + 0.0088C + 0.054C^{2/3} + 0.036C_{ss}$$

Phytoplankton reaction to light.

The rate of the light reaction of photosynthesis is strictly dependent on light intensity. Increases in light intensity lead to greater photosynthetic rates until some maximum is reached. At this point the producers cannot use any more light, the enzymes involved in photosynthesis cannot act fast enough to process light quanta any faster, so rate of photosynthesis reaches an asymptote. Increasingly higher light intensities usually inhibit photosynthesis (Valiela, 1995).

During the last decades a considerable amount of research has been carried out on primary productivity modelling (e.g. Steele, 1962; Jassby and Platt, 1976; Platt *et al.*, 1980; Falkowski & Wirick, 1981; Eilers and Peeters, 1988). In most of these works formulations of the relationship between primary productivity and light intensity were proposed and tested against field and/or laboratory data. Most of these equations are empirical, only a few of them being deduced from the physiology of photosynthesis (e.g. Fasham and Platt, 1983; Eilers and Peeters, 1988). These formulations have been used for several years in ecological models.

The light intensity affects only the photosynthesis, its representation use the formulation of Steele (1962) integrated on the depth, Parsons *et al..*, (1995) for this zero-dimensional model and a classic Beer-Lambert function for the light intensity.

$$E(z) = E_0 \cdot e^{(-k(p)z)}$$

$$\Psi(E) \ = \frac{e^1}{k(p).z} \cdot \left(e^{-\frac{E_0}{E_{opt}} e^{(-k(p).z)}} - e^{-\frac{E_0}{E_{opt}}} \right)$$

With: E_0 : effective solar radiation at the water surface (W.m^{-2}); $k(p)$ is the light extinction factor (m^{-1}); E_{opt}: optimal light intensity for photosynthesis, z : depth (m).

Ecological model equations

The Ecological model has been developed in terms of sinks and sources. Such an approach is convenient to give these models the desired flexibility, providing it with the capability of being coupled to either a Lagrangian or a Eulerian resolution method.

Because of the properties interdependency a linear equation system is computed for each control volume and this system can be compute forward or backward in time.

The simulation of the water quality processes is developed with the following considerations: Autotrophic producers consume inorganic nutrients and depend on both their availability and sunlight as a source of energy for photosynthesis. Nitrate and ammonia are the inorganic nitrogen forms that primary producers consume. The Primary and Secondary producer's excretions are considered, acting as source for the nitrogen cycle. Primary producers are consumed by secondary producers, which in turn are consumed by higher trophic levels.
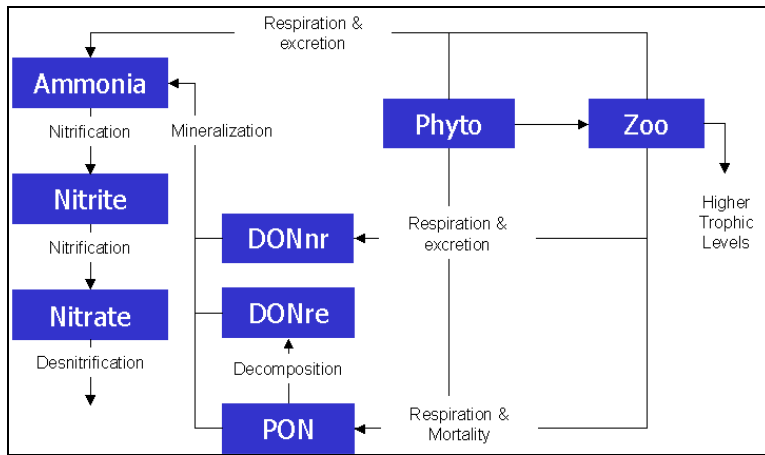
Figure 4 conceptual model scheme.

Phytoplankton

Phytoplankton is described in terms of carbon concentration (mg C l^{-1}). The model assumes three limitations affecting the maximum phytoplankton growth rate (μmax): Temperature $\Psi(T)$, light effect $\Psi(E)$ and nutrient limitation $\Psi(N)$. Respiration of phytoplankton is divided into two parts, dark respiration and photorespiration. A large proportion of phytoplankton photosynthates can be released into the water as extracellular dissolved organic material (DONnr). Excretion rate is influenced by the light limitation factor (Collins, 1980). The non-grazing mortality uses a modified Michaelis-Menten formulation proposed by Rodgers and Salisbury (1981).

Phytoplankton equations

$$dPhy/dt = (\mu_{Phy} - r_{Phy} - ex_{Phy} - m_{Phy}).\ Phy - G$$

Process	Symbol	Unit	Equation
Growth	μ_{Phy}	d^{-1}	$\mu_{Phy} = \mu_{max} .\ \Psi(N)_{Phy} .\Psi(E)_{Phy} .\Psi(T)_{Phy}$

Respiration	r_{Ph}	d^{-1}	$r_{Phy} = k_{er} \cdot \exp(0.069 \cdot T^\circ) + k_p \, \mu_{Phy}$
Excretion	ex_{Ph}	d^{-1}	$ex_{Phy} = \varepsilon_{Ph} \cdot \mu_{Ph}(1 - \Psi(E)_{Ph})$
Natural mortality	m_{Ph}	d^{-1}	$m_{Phy} = m_{max/Phy} \cdot \dfrac{\dfrac{Phy}{\mu_{Phy}}}{Km + \dfrac{Phy}{\mu_{Phy}}}$
Grazing	G	mgC/ld	$G = \dfrac{g_z}{E} Zo$

Table 3 Rates and equations for the phytoplankton variable

	Symbol	Coefficient	Unit	Value
	μ_{max}	Maximal growth Rate	d^{-1}	2.2
	ε_{Phy}	Excretion constant	-	0.07
	k_{er}	Endogenous respiration constant	-	0.0175
	k_p	Photorespiration factor	-	0.125
	K_m	Mortality half saturation rate	mgC.d.L^{-1}.	0.3
	m_{max}	Maximal mortality rate	d^{-1}	0.02
	E	Assimilation efficiency		0.6
Nutrient limitation	K_N	Half saturation constant for nutrient limitation	mgN.L^{-1}	0.014
Temperature limitation $Topt_{min}Phy$		Minimal temperature for an optimal photosynthesis	ºC	25.0
	$Topt_{max}Phy$	Maximal temperature for an optimal photosynthesis	ºC	26.5
	$Temp_{min}Phy$	Minimal temperature for photosynthesis	ºC	4.0
	$Temp_{max}Phy$	Maximal temperature for photosynthesis	ºC	37.0
	$Eopt$	Optimal light intensity for photosynthesis	Wm^{-2}	100
	α_{Phy}	Redfield ratio (N:C)	-	0.18
	$K_{PhyNutReg}$	phytoplankton nutrient regeneration half saturation rate	mgN.L-1	1.0
	$F_{org\,P/Ph}$	Fraction of organic particulate excretion		0.7
	$f_{in/Phy}$	Fraction of inorganic excretion	-	0.5
	$f_{orgD/Phy}$	Fraction of organic soluble excretion	-	0.4

Table 4 Values used in the standard model for the phytoplankton variable

Zooplankton

Zooplankton is described in terms of carbon concentration (mg C l^{-1}).

The net growth rate (day^{-1}), g_z is obtained from Ivlev, (1945) adapted by Parsons *et al.*, (1967). Respiration and non-predatory mortality of the zooplankton (day^{-1}), r_z and m_{Z0} are considered functions of temperature, being treated as one variable. The predatory mortality, G_z, depends on the zooplankton concentration.

Zooplankton equations

$$d\,\mathbf{Zo}/dt = (g_z - r_z - m_{Z0})\,.\,\mathbf{Zo} - G_z$$

Growth	g_z	d^{-1}	$g_z = g_{max}\left(T_{ref}\right)\Psi(T)\left(1 - e^{-\Lambda(Phy - Phy_0)}\right)$
Natural mortality + respiration	$r_z + m_{Z0}$	d^{-1}	$r_Z + m_Z = d_Z(T_{ref})\Psi(T)$
Grazing	G_z	mg C/ ld	$G_z = e_z Z$

Table 5 Rates and equations for the zooplankton variable

	Symbol	Coefficient	Unit	Value
	g_{max}	Maximal growth Rate	d^{-1}	0.1
	Δ	Ivlev constant	-	13.0
	Phy_0	Minimum phytoplankton concentration for grazing	mgC/l	0.045
	d_z	Non predatory mortality and respiration rate	d^{-1}	0.036
	ez	Predatory mortality rate	d^{-1}.	0.01
Temperature limitation $Topt_{min}Zo$		Minimal temperature for an optimal zoo growth	ºC	24.8
	$Topt_{max}Zo$	Maximal temperature for an optimal zoo growth	ºC	25.1
	$Temp_{min}Zo$	Minimal temperature for zoo growth	ºC	5.0
	$Temp_{max}Zo$	Maximal temperature for zoo growth	ºC	35.0
	α_{Phy}	Redfield ratio (N:C)	-	0.18

Table 6 Values used in the standard model for the zooplankton variable

Nitrogen

In the present model, nitrogen is represented in different forms namely: the organic forms, particulate organic nitrogen (**PON**) and dissolved organic nitrogen (**DON**).

This variable is divided in dissolved organic nitrogen non refractory (**DONnr**), including small molecular substrates, assumed to be degraded in the day of production, and the dissolved organic nitrogen refractory (**DONre**) with a longer turn over. And the inorganic forms: dissolved inorganic nitrogen (**DIN**). This variable is divided in 3 components: ammonia (NH_4), nitrite (NO_2) and nitrate (NO_3).

To simplify the equation (already complex) we assumed than the variable: *Phy', Zo'* represent respectively the phytoplankton, and zooplankton expressed in nitrogen unit ($mgN.L^{-1}$), this transformation is obtained with the corresponding N:C ratio (α_x).

Nitrogen Equations

$$\frac{d\,PON}{dt} = [(1 - f_{orgD\,/Ph})(1 - f_{in/Ph}).e_{Ph} + m_{Phy}\,].\textbf{\textit{Phy'}} + [(1 - f_{orgD\,/Zo})(1 - f_{in/Zo}).e_{Zo} + m_{Zo} + \delta_{Zo}]\,.\textbf{\textit{Zo'}}$$

$$+ - \varphi_{det}\,\textbf{\textit{PON}}$$

$$\frac{d\,\textbf{DONnr}}{dt} = f_{orgD/Ph}\,(1 - f_{in/Ph}).e_{Ph} + f_{orgD/Zo}.(1 - f_{in/Zo}).e_{Zo}\,.\textbf{\textit{Zo'}} - \varphi_{Nnr}\,\textbf{DON}_{nr}$$

$$\frac{d\,DONre}{dt} = \varphi_{det}.\textbf{PON}(1 - F_{org\,P/Ph}) - \varphi_{Nr}\,\textbf{DONr}$$

$$\frac{d\,NH_4}{dt} = f_{in/Fs}.e_{Ph}.\textbf{\textit{Phy'}} + f_{in/Zo}.e_{Zo}.\textbf{\textit{Zo'}} - \Phi_{NH4} - \varphi_{2N}.\textbf{\textit{NH4}} + \varphi_{Nr}\,\textbf{DONr} + \varphi_{Nnr}\,\textbf{DONnr}$$

$$+ f_{org\,P/Ph}\,\varphi_{det}\,\textbf{PON}$$

$$\frac{d\,NO_2}{dt} = \varphi_{2N}.\textbf{NH}_4 - \varphi_{2N}.\textbf{NO}_2$$

$$\frac{d\,NO_3}{dt} = \varphi_{2N}.\textbf{\textit{NO2}} - \Phi_{NO3} - \varphi_{3N}.\textbf{\textit{NO3}}$$

Table 7 Equations for the nitrogen variable

Symbol	Process	Construct
Φ_{NH4}	Photosynthetic assimilation for NH_4	$\Phi_{NH4} = \beta_{NH4}.\alpha_{Phy}.\mu_{Ph}$

Symbol		Coefficient		Equation

β_{NH4} — Ammonia preference factor of phytoplankton

$$\beta_{NH4} = \frac{NH_4 . NO_3}{(K_N + NH_4)(K_N + NO_3)} . \frac{NH_4 . K_N}{(K_N + NH_4)(K_N + NO_3)}$$

Φ_{NO3} — Photosynthetic assimilation for NO_3

$$\Phi_{NO3} = (1-\beta_{NH4}).\alpha_{Phy}. \mu_{Ph}$$

φ_{2N} — Nitrification rate

$$\varphi_{2N} = M_{nitri} . \theta_{nitri}^{(T-Tref)} . \frac{O_2}{Knitri + O_2}$$

φ_{det} — PON dissolution

$$\varphi_{det} = M_{det} . \theta_{det}^{(T-Tref)}$$

φ_{Nnr} — DONNonrefractory mineralisation rate

$$\varphi_{Nnr} = M_{DON}(T_{ref}) \theta_{DON}^{(T-Tref)}$$

φ_{Nr} — DONrefractory mineralisation rate

$$\varphi_{Nr} = M_{DONre} . \theta_{DONre} (T-Tref) . \frac{Ph}{KPhNutRege + Ph}$$

φ_{3N} — Denitrification rate

$$\varphi_{3N} = M_{denit} . \theta_{denit}^{(T-Tref)} . \frac{Kdetri}{Kdetri + O_2}$$

Table 8 Processes represented in the model for the six nitrogen state variables

Symbol	Coefficient	Unit	Value
T_{ref}	Reference temperature	^oC	25
M_{DONre}	Reference rate for mineralization	d^{-1}	0
M_{DONnr}	Reference rate for mineralization	d^{-1}	0.1
θ_{DONre}	Temperature coefficient for mineralization of DONre	-	1.02
θ_{DONnr}	Temperature coefficient for mineralization of DONnr	-	1.02
$K_{PhNutRege}$	Half saturation constant for phytoplankton regeneration	-	1.
M_{nitri}	Reference rate for nitrification		0.1
θ_{nitri}	Temperature coefficient for nitrification	-	1.08
K_{nitri}	Half saturation constant for nitrification		2.0
M_{det} .	reference rate for PON dissolution	d^{-1}	0.1
θ_{det}	Temperature coefficient for decomposition	-	1.02
M_{denit}	reference rate for denitrification	d^{-1}	0.1
θ_{denit}	Temperature coefficient for denitrification	-	1.046
K_{denit}	Half saturation constant for denitrification	$mgO_2.L^{-1}$	0.1
α_{Phy}	N:C ratio for phyto	-	0.18
α_{Zo}	N:C ratio for zoo		0.24

Table 9 Values used in the standard model for the nitrogen variables.

V. Results and Conclusions

Numerical tool description (MOHID 2000)

MOHID2000 is a full 3D-baroclinic model and has been developed using an object oriented programming philosophy and using all the FORTRAN 95 potential. The system has two main classes: the first one manages the hydrodynamic properties (e.g. velocity, elevation, water fluxes, turbulent viscosity) and the second one the water properties (e.g. salinity, temperature, density, SPM, nutrients, phytoplankton, coliforms).

The model is based on a finite volume concept. In this approach the discrete form of the governing equations are applied macroscopically to the cell control volume in the form of flux divergence. As a consequence this method automatically guarantees the conservation of transported properties (Adcroft et al., 1997).

The hydrodynamic properties evolution is computed solving the three-dimensional primitive equations in rectangular co-ordinates for incompressible flows. Hydrostatic equilibrium is assumed as well as Boussinesq approximation. The turbulent viscosity can be computed using several models. In the horizontal the options are constant value or Smagorinsky models. In the vertical the models that can be used are: a constant value, a mixing length model (Nihoul, 1984), a one-equation (K) model or a two-equations (K-L) model (Gaspar, 1990). The water properties evolution is computed solving the advection diffusion equation explicitly in the horizontal and implicitly in the vertical. The sinks are computed forward in time and the sources are computed backwards to avoid negative values of mass.

The system can make use of five different types of boundary conditions: free surface, bottom, lateral closed boundary, moving boundary and lateral opened boundary (Santos and Neves, 1991). Moving boundaries are closed boundaries whose position varies with time. For the lateral and moving boundaries the conditions are always null flux. Any exchange between land and the sea is computed as a discharge (for example a river or an outfall). The discharge class can compute the discharges of hydrodynamic properties (ex: momentum) and also of water properties (ex: SPM, salinity). For each of the other three boundary conditions: bottom, surface and open boundary, there are specific classes. The bottom class is responsible for the fluxes between the bottom and the water column (*e.g.,* shear friction, erosion/deposition of sediments). The surface class is

responsible for the fluxes between the atmosphere and the water column (*e.g.,* wind forcing, gas emission, solar radiation).

A model is more than a program that uses a set of algorithms to solve a set of equations. A model with only good equations and good algorithms is not able to grow in orderly way. To avoid chaotic growth it is necessary to implement program techniques that ensure reliability and maintainability. The object-oriented programming is the most powerful technique to achieve these goals. This issue is especially important for large software systems like the MOHID 2000. These systems are usually developed by several collaborators separated in space and in time and for this reason a model must be able to incorporate new contributions always with a smiling face.

Another very important issue is the input data (pre-processing) of complex models like this one. It's necessary to develop graphical interfaces to help users to give the necessary data in a systematic way to the model. If the user does not belong to the development team the probability of introducing input data mistakes is high if the input data methodology is for example Ascii files. Output data (post-processing) analysis is also an important issue especially when you are talking of a 4D numerical tool (3 spatial dimension plus time) that is able of computing the evolution of almost 30 properties. If the users do not have access to tools that allows them of seeing the output data in an intuitively way this task can lead to madness. A graphical interface was developed to allow the user to explore the data using 2D images (3D slices) animated in time.

Analise Tools

Usually, to study a property's temporal variation, we compute a time series in some point of the domain. Nevertheless, a question emerges, is the chosen point representative of the whole area? This creates a serious dilemma if we want to extrapolate conclusions about spatial variation. By the other hand the best way to look at spatial variation it's plotting the property's field at some time instant. By assembling different time instants maps in a sequence, it becomes possible to look at spatial and temporal variation together. Although this "global" result can be quite satisfying, it may not be yet the ideal, if our goal is to look at characteristics of particular areas in the estuary. In that case the ideal solution must be one in which after defining the distinct areas, we integrate the results computed for each cell of that particular area. This conclusion leads us to the concept of Integration Boxes. With this method its possible,

not only, to know the average property's value in each area defined by the box, has well to compute the properties fluxes between boxes, which give us a great insight into the dynamical processes in the estuary. With this method it becomes easy to determine and calibrate the energy fluxes between the subsystems, and to reach for more accurate answers from a quantitative point of view about the changes caused to the habitat by each simulation scenario.
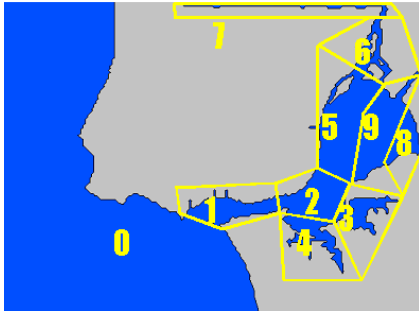
Figure 5 – Boxes definition in the Tagus estuary

Tagus estuary application

Introduction (adapted from Vale e Sundby, 1987)

The Tagus estuary is the largest Portuguese estuary and one of the largest European estuaries, located near Lisbon (38º44'N, 9º08'W) and covering na area of about 300 km^2 at low tide and 340 km2 at extreme high tide. The estuary is composed of a deep, straight and narrow inlet channel and a broad, shallow inner bay. The inlet channel, allowing the entrance of seawater in the estuary, is about 15 km long and 2 km wide, while the bay is about 25 km long and 15 km wide. Upstream, a single narrow channel marks the entrance of the Tagus river. The morphology of the Tagus estuary fits better into the category of tidal lagoons, as defined by Dronkers and Zimmerman (1982). It is a mesotidal estuary and the tides are semi-diurnal, with a tidal range in Lisbon varying from about 1m at neap tide to about 4 m at spring tide. The tidal effect reaches 80 km landward od Lisbon. The tidal wave is progressive, and at spring tide the high water is delayed by as much as two hours between Lisbon and Vila Franca. The subtidal volume of the estuary. The residence time of fresh water is highly variable and ranges from 65 days at a discharge of 100 m^{3}s^{-1} to 6 days at a discharge of 2200m^{3}s^{-1} (Martins *et al.*, 1984).

The Tagus is the main source of fresh water of the estuary and its discharge pattern clearly reflects the dry and wet seasons. The average annual discharge varies between 80 and 720 m^3s^{-1} and the average monthly discharge may vary between 1 and 2200 m^3s^{-1} (Loureiro, 1979).

Hydrodynamic processes

The Tagus estuary hydrodynamic calibration has been done in the framework of other projects (OPCOM and SANEST) and was been the subject of a PhD. thesis. In this report only some results to illustrate the main features of the Tagus estuary hydrodynamic are presented.

Residual velocities presented in Figure 6 (surface values) were obtained through time integration of transient velocities. Residual velocities do not usually provide much direct information but they can be helpful to understand long-term phenomena with time scales much larger than the tidal period. There is a jet outward the estuary associated with a strong anticyclone off Costa do Estoril; a cyclone and an anticyclone inside the channel reveals a very complex hydrodynamic system coupled with the topography.

Figure 7 shows instantaneous surface velocities during ebb (5h 44m after high water, tide amplitude 3m). The maximum velocity occurs in the channel. This figure shows the Cascais' bay periodic anticyclone (it appears during ebb time) and the outward jet. These features, also visible in the residual velocity (Figure 6) have a strong influence in the bathing coastal area of Cascais; because of this gyre the estuarine ebb water weakly affects the area. Model results (and other field studies) strongly suggest that water quality in this area depends first of all on the proper control of local pollution sources.
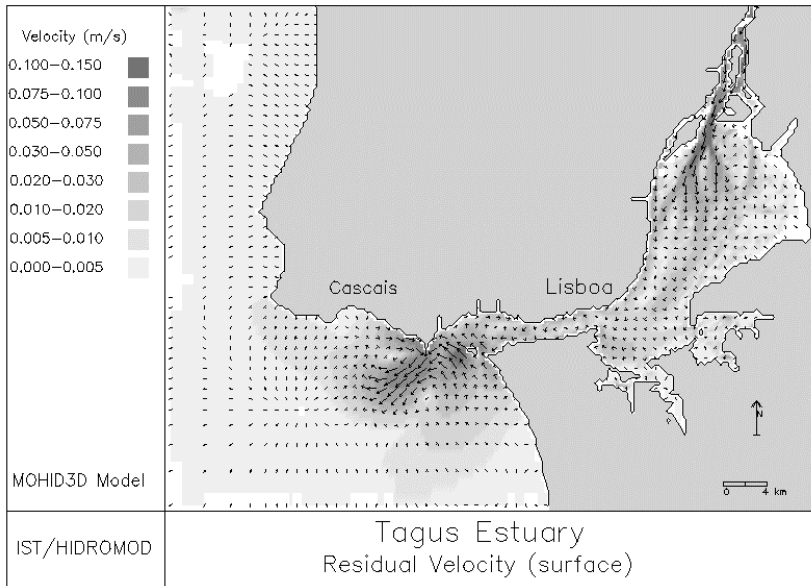
Figure 6 - Tagus Estuary surface residual velocity field.
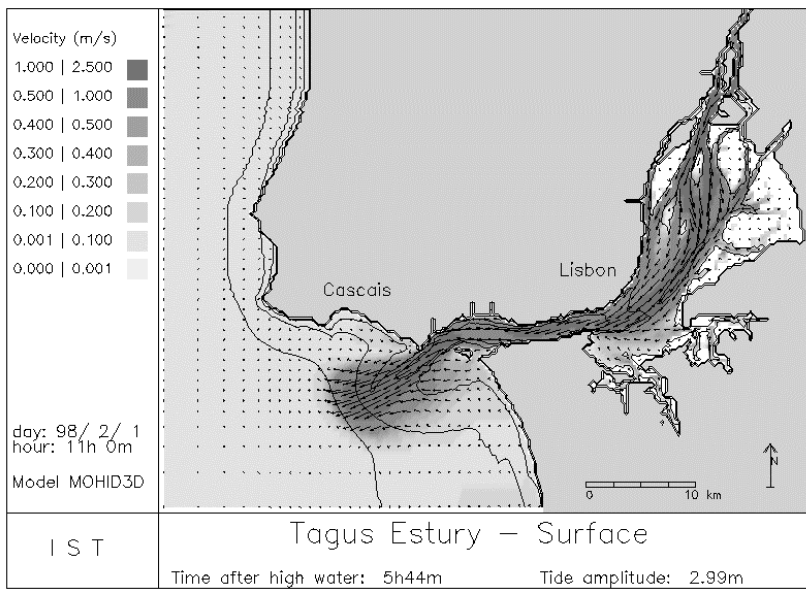
Figure 7 - Transient velocity field.

Cohesive sediment processes

The work that follows comes in the sequence of the studies on the calibration of the eulerian sediment transport model (Clipper, 1998). Previous results confirm that the Tagus estuary is characterized by considerable fortnightly and semi-diurnal fluctuations in turbidity, caused by a cyclic variation in strength of the bottom currents, which determines the erosion - deposition cycle, in particular of the large intertidal areas (about 40 % of the estuary) and the intensity of the turbidity maximum, located in the

upper estuary. One of the conclusions of Clipper, (1998) is that the formation of the turbidity maximum is principally produced by barotropic effects. This effect may be amplified by the residual flow associated to the density gradient (net flow upstream in the lower layer, net flow downstream in the upper layers).

Although the obvious importance of the fortnightly cycle in the sediment transport, all the simulations were done considering the semidiurnal cycle only. The tradeoffs of this methodology were already explained and it should be noticed that the aim here is not to enter in a deep study about sediment transport but simply to compute the sediment field concentrations that will determine the light regime that consequently will affect primary production.

Nevertheless the results obtained show good consistency with average field data and represent a step forward in the developing of sediment transport in the MOHID modeling system by introducing the wave effect on resuspension.

Initial and boundary conditions

The Tagus river is the source supply of sediments to the estuary, a constant discharge concentrations of 100 mg/l (Portela, 1996) was considered. Sediment water column concentration as its sink term on deposition and source term on erosion from bottom accumulated sediments. The initial bottom accumulation is the results of a previous simulation that began with a constant value for bottom accumulation and then waited for hydrodynamics to do its job, this means to take out sediments form erosion areas, deposit it on deposition areas and transport to the continental shelf the excess concentration. This methodology is carried out until an equilibrium situation is established, that happens when water column concentrations and bottom accumulations have small residual changes.

Influencing parameters

Previous studies show that the most influencing parameters on the sediment transport model are critical sheer stress of erosion and deposition (τ_E, τ_d), and the m exponent on the settling velocity equation. On this study a new set of parameters that controls the sheer stress caused by waves is introduced: the wave high, W_h, (m) and wave period, W_p (sec.).

M parameter

As already explained the settling velocity can be determined by

$$W_S = K_1 C^m \qquad\qquad\qquad \text{for } C < C_{HS}$$

$$W_S = K_1 C_{HS}{}^m \left[1.0 - K_2 (C - C_{HS})\right]^{m_1} \quad \text{for } C > C_{HS}$$

where W_S (ms^{-1}) is the settling velocity, C (kgm^{-3}) is the concentration, and the subscript HS refers to the onset of the hindered settling (4 kgm^{-3}). The coefficients K_1 (0.006 m^{4}kg^{-1}s^{-1}) and K_2 (0.1 m^{3}kg^{-1}) depend on the mineralogy of the mud and the exponents m(2.0) and m_1(2.0) depend on particle size and shape. These parameters were calibrated for the Tagus estuary in Clipper, (1998) for fortnightly cycle conditions.

The next figure shows how that increasing the m parameter results in the diminution of the settling velocity for different sediment concentrations. This fact explains the results presented in Figure 11 and Figure 12.
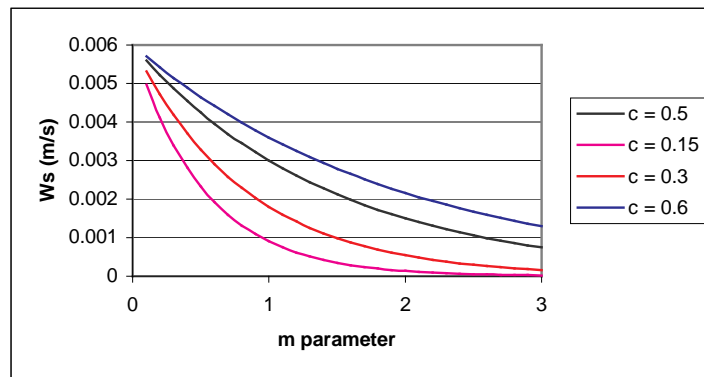
Figure 8 Settling velocity variation with m parameter for different sediment concentrations (kg/m3)

The next figures show the obtained result for two runs both with no waves and the same constrains (.τ_e = 0.6 Pa, τ_d = 0.3 Pa), except the m parameter. In run G1, m=3.0 and in run F1, m=2.0. Figure 11 shows average sediments concentration over a year in different locations all over the estuary (see Figure 9). It is clear the values are consistently higher for run G1 (50 % on average over all field stations). This could be explained by the fact that with a lower m value the settling velocity is higher in run F1 then there will be much more deposition so the sediment concentration in the water column will decrease comparing to run G1. In terms of fluxes (Figure 12) the increased water column concentrations of Run G1 causes also increased fluxes between boxes that surround major pathways of sediments (Boxes 6,5,2 and1). Among the remaining boxes, 9,8 4 and 2 that surround mostly the intertidal areas, a change in the m parameter

causes the inversion of the fluxes direction. This is especially relevant between boxes 5 and 9 because box 9 is known to be a deposition area so a inflow of sediments from box 5 is much more logical then a outflow. Nevertheless looking again to Figure 11 and comparing the obtained results to the ones measured by Martins e Duffner (1982) for the same locations, run G1 is more accurate besides this both runs show less accuracy in field stations 3.0 and 2.5. We should notice that these points are located in intertidal areas where in a typical windy day small waves occur. The waves act as a destabilization, mobilization and suspension factor for the sediments so this could be the reason to the increased water column concentrations.

.

Figure 9 Field stations location

Figure 10 Boxes definition in the Tagus estuary

Figure 11 Sediments concentration for run F1 (m=2.0) and run G1 (m=3.0) and no waves

Figure 12 Sediment fluxes between integration boxes for run F1 (m=2.0) and run G1 (m=3.0) and no waves
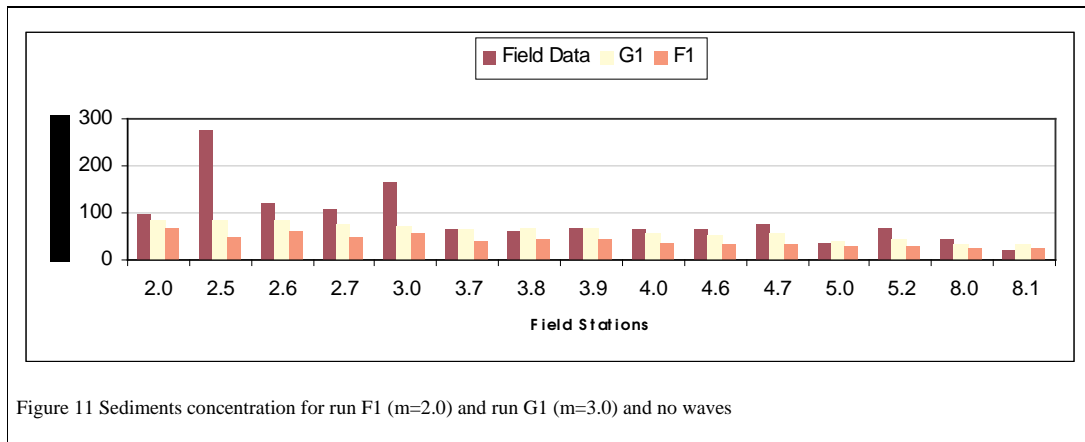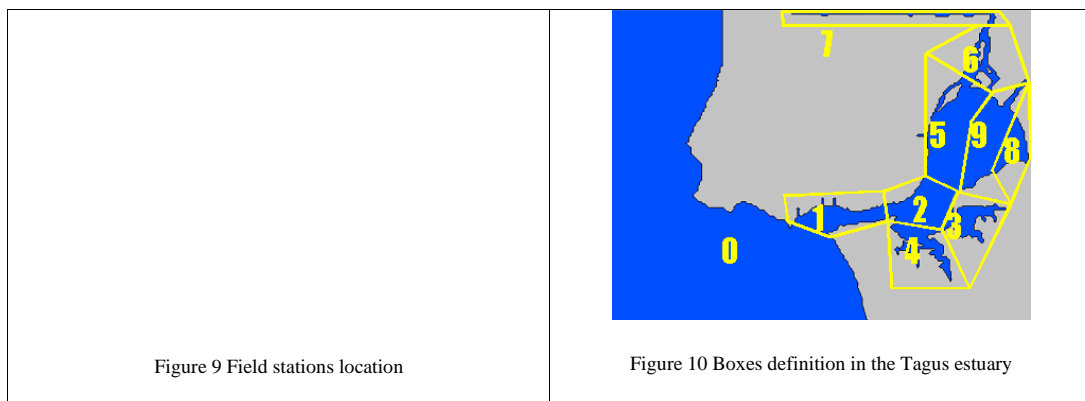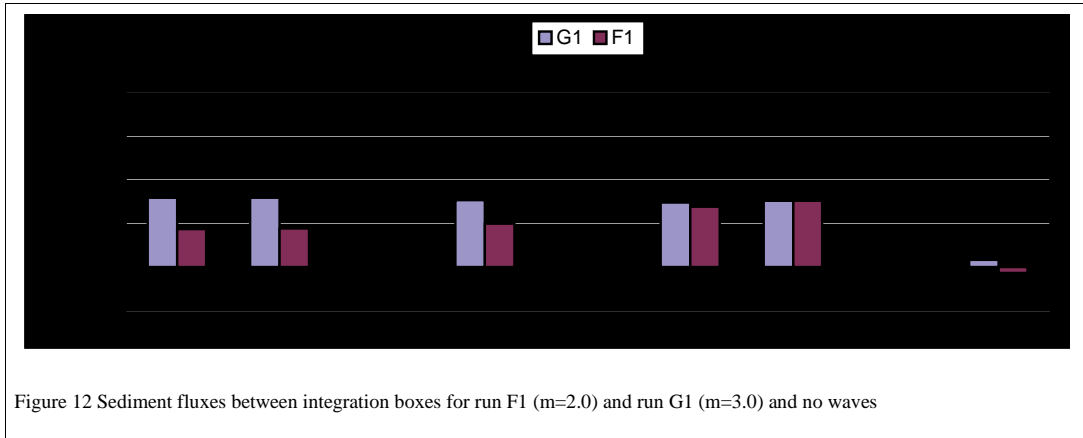
Waves and critical sheer stress

Resuspension is taken to be related to both wave and current induced bottom stress. In some research studies especially applied to shallow lakes, wind-induced waves are known to dominate the resuspension process such that the effect of the current is neglected (Somlyódy and Koncsos, 1991) .On the other hand, it is well established that the resuspension process and gross sediment transport processes in rivers depend heavily on the flow characteristics. The waves act as a destabilization, mobilization and suspension factor for the sediments, and a minimal current may be able to carry away the already activated sediment grains. In essence, the effect of both current and waves in the sediment resuspension and transport process can be viewed as inseparable (Rivera, 1997). These surface waves riding atop the tide and wind-generated surface elevation, have a period scaled in seconds, and small highs.

The inputs parameters for the wave model are wave period, W_p (sec.) and wave high, W_h (m). Bottom shear stress is directly proportional to wave high and indirectly proportional to wave period. These parameters were imposed to boxes 8 and 9 where small depth and wind contribute to the commonly observed waves in those areas.

The next figures show the results from G1 with waves and Run G2 with waves.
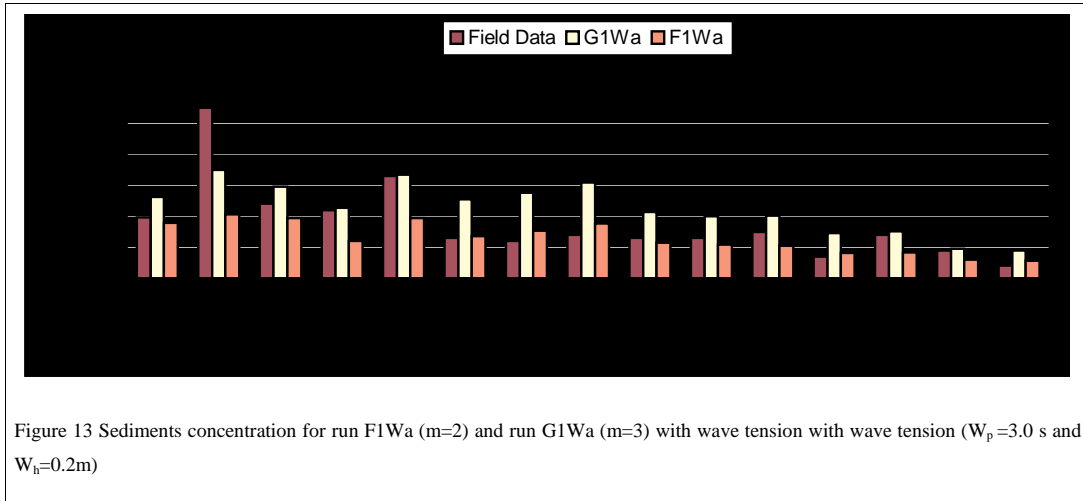
Figure 13 Sediments concentration for run F1Wa (m=2) and run G1Wa (m=3) with wave tension with wave tension (W_p =3.0 s and W_h=0.2m)
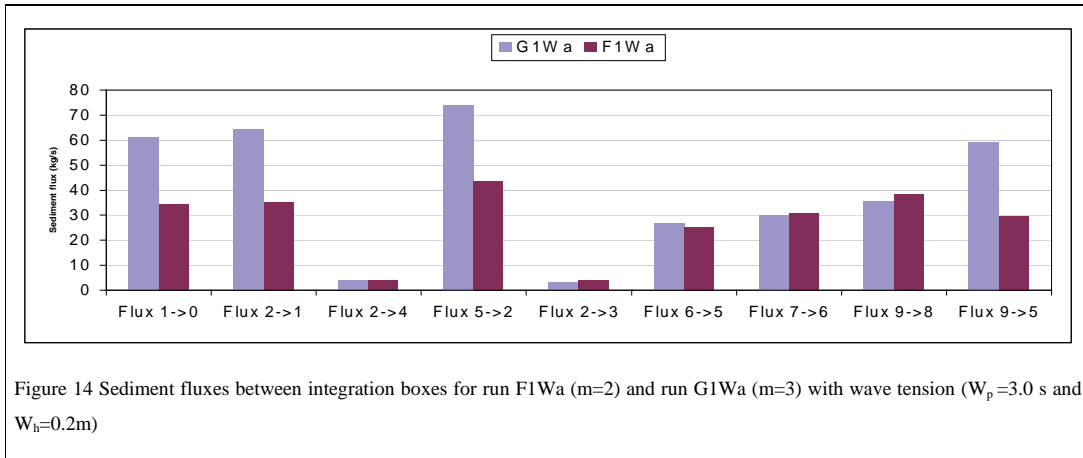
Figure 14 Sediment fluxes between integration boxes for run F1Wa (m=2) and run G1Wa (m=3) with wave tension (W_p =3.0 s and W_h=0.2m)

Both concentration and consequently sediment fluxes increase in all stations with the introduction of this destabilization factor. Average results over all field stations show a difference between G1 and G1Wa of 81% and between F1 and F1Wa of 56% so we can conclude that both factors waves and m exponent (affecting settling velocity) act together do increase water column concentrations. This was already expected, waves increase the erosion process and lower settling velocity diminishes deposition so we have an increased sediment water column concentration and decreasing bottom accumulation. Although these values show the average results integrated over a year, this is not by all means a stable situation because the water column input will only be maintained until bottom accumulation in boxes 8 and 9 extinguish.

Again we should not forget that the aim in this application is to simulate sediment concentration in the water column, in order to compute the extinction coefficient of light in water that consequently will affect photosynthesis and primary

production. The results obtained are consistent with this objective. Figure 15 shows average sediment water column concentration measured and simulated. Although the model underestimates concentrations in every field station, it's able to qualitatively simulate with great accuracy sediment distribution in the estuary. This result allows determining the areas where light extinction will exert the most influence.

Further developments in this study area should include the fortnightly cycle but also to maintain the adequate simulation time scale to support water quality modeling.

Figure 15 Sediments concentration for m=2 with wave tension (W_p=3.0 s in box 8 and W_p=10.0 s in box 9 and W_h=0.2m)
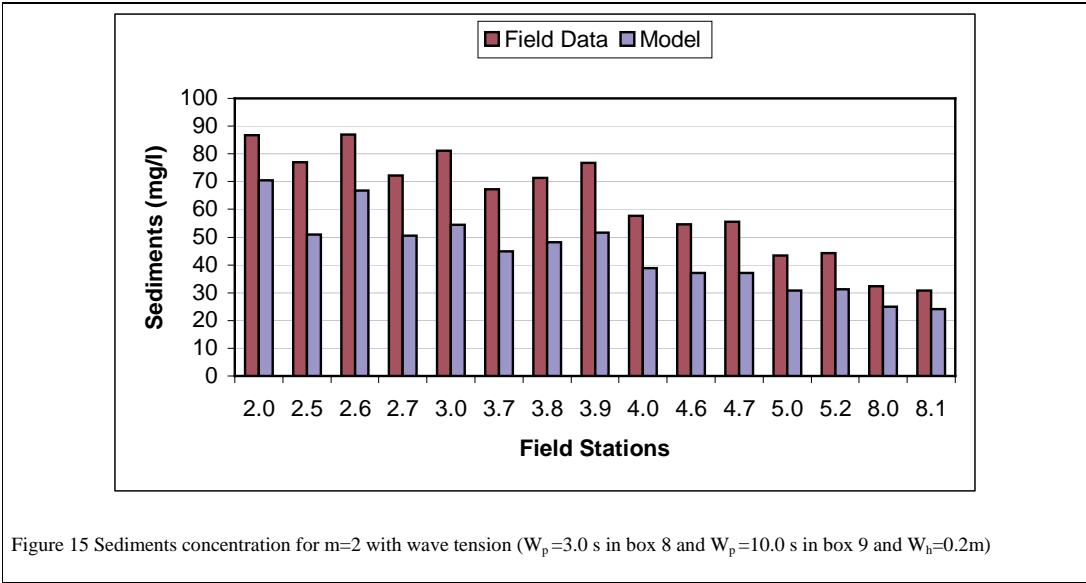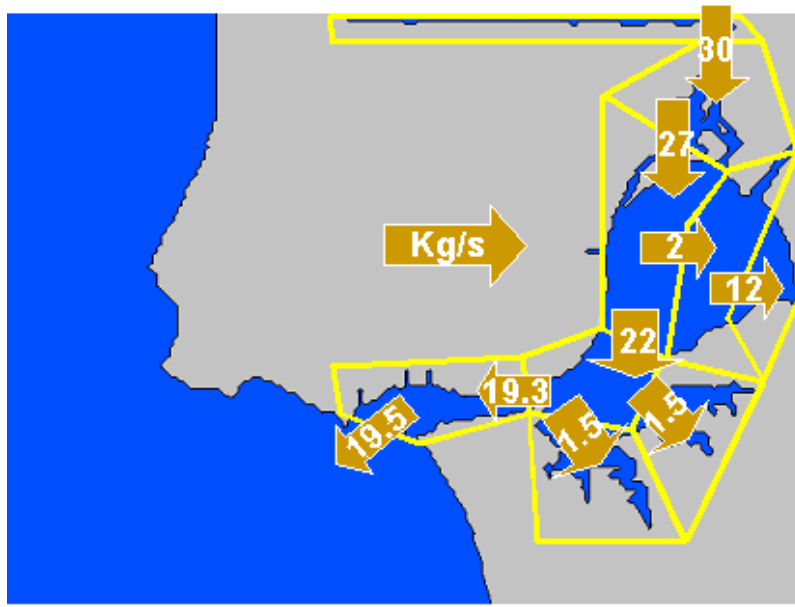
Figure 16 Sediments fluxes for m=2 with wave tension (W_p=3.0 s in box 8 and W_p=10.0 s in box 9 and W_h=0.2m)

Water quality processes

Initial conditions

The values for the initial concentrations of phytoplankton defined for each box where established after average analysis from accountings in the Tagus estuary over several years described in the bibliography (Portela, 1996; Antunes, 2000). The average river flow considered was 300 m^3s^{-1} (Antunes, 2000) and the river discharge concentrations where obtained from INAG's data base (www.inag.pt) and Antunes, (2000).

BOX	1	2	3	4	5	6	7	8	9
Phytoplankton (mg C/L)	0.07	0.06	0.04	0.08	0.17	0.26	0.19	0.17	0.17
Zooplankton (mg C/L)	0.007	0.006	0.004	0.008	0.017	0.026	0.019	0.017	0.017
Nitrate (mg N L^{-1})	0.13	0.17	0.18	0.28	0.37	0.41	0.49	0.37	0.37
Nitrite (mg N L^{-1})	0.01	0.01	0.02	0.02	0.02	0.01	0.00	0.02	0.02
Ammonia (mg N L^{-1})	0.05	0.11	0.13	0.28	0.28	0.12	0.03	0.12	0.12
PON (mg N L^{-1})	0.13	0.19	0.21	0.38	0.44	0.35	0.35	0.38	0.38
DONnr (mg N L^{-1})	0.05	0.05	0.06	0.05	0.03	0.03	0.02	0.03	0.05

Table 10 Initial concentrations in each box (see Figure 5 for boxes definition)

	Discharge concentration
Phytoplankton	0.10 (mg C L^{-1})
Zooplankton	0.01 (mg C L^{-1})
Nitrate	0.60 (mg N L^{-1})
Nitrite	0.03 (mg N L^{-1})
Ammonia	0.45 (mg N L^{-1})
DONnr	0.20 (mg N L^{-1})
PON	0.20 (mg N L^{-1})

Table 11 Concentrations on river discharge

We assume that the concentration of chlorophyll-a is directly proportional to the concentration of phytoplanktonic biomass (Valiela, 1995). The conversion factor is usually in the range of 20-100 mgC/mg Chlorophyll –a depending on phytoplankton class and nutritional state (Kramer *et al*, 1994). Portela (1996) determine by linear regression a conversion value of 60 mgC/mg Chlorophyll for the Tagus estuary

Sensitivity analysis

A sensitivity analysis was carried out to study the extent to which uncertainties in the values of parameters influence the equilibrium values of phytoplankton and zooplankton biomass. The methodology chosen was to change separately some model parameters and measuring the response to the state variables relatively to a reference situation (see Table 4, Table 6 and Table 9). The sensitivity analysis was focused on the most uncertain parameters of the model that were estimated from the calibration procedure. Each model parameter was reduced at half and then increased twofold and the percentage changes of phytoplankton and zooplankton biomass were estimated.

Symbol	Coefficient	Twofold increase		Half reduction	
		Phy [%]	Zoo [%]	Phy [%]	Zoo [%]
μ_{max}	Phy. maximal growth rate	a	a	-62.1	-64.3
K_m	Phy. mortality half saturation rate	1.3	1.7	-1.1	-1.4
m_{max}	Phy. maximal mortality rate	-19.0	-20.0	11.9	12.8
ε_{Phy}	Phy. excretion constant	-9.8	-10.4	3.8	3.9
K_N	Nitrogen half saturation constant	-2.6	-2.4	2.7	2.6
ez	Zoo predatory mortality rate	52.3	-34.9	-12.3	22.7
g_{max}	Zoo maximal growth rate	-67.3	22.5	99.1	-74.6
d_z	Zoo non predatory mortality and respiration rate	88.5	-70.9	a	a
Eopt	Optimal light intensity	- 34.4	-38.6	30.3	42.9

for photosynthesis	

Table 12 Sensitivity evaluation for phytoplanktonic and zooplanktonic biomass; percentage changes induced after twofold increase and half reduction of model parameters.

[a] numeric instability

In this set of parameters, undoubtedly, phytoplankton maximal growth rate and zooplankton non predatory mortality and respiration rate represent the most influencing parameters. The first controls phytoplankton exponential growth and the second represent the major sink to zooplankton development. In this test we went beyond the reasonable limits to these parameters that cause a numeric instabilization of the model. The reciprocal parameters, phytoplankton excretion and zooplankton maximal growth doesn't cause the some effect on phytoplankton and zooplankton biomass because their growth in this case is limited. Phytoplankton can have a low excretions term because it's increase will be controlled by the subsequent zooplankton growth due to heavy grazing. On the other hand zooplankton growth is only possible if phytoplankton is present so its large growth rate can only be maintained until a certain point. The test done on zoo grazing by higher trophic (ez) enhances this last conclusion, for half reduction we can see significant changes on both state variables. Due to less zooplankton, phytoplankton will be able to growth. With twofold increase the changes are not so dramatic mainly because although zooplankton has more potential to growth it is limited by phytoplankton concentration. Optimal light intensity (*Eop)* is also an relevant parameter, it affect directly phytoplankton threw light limitation and indirectly zooplankton threw available food.

Results

The following results show time series comparisons between model and field data from the Tagus Field Station 3.5 after Martins & Dufner (1982), Martins *et al.* (1983a, 1983b) and Silva *et al.* (1986a), for four consecutive years: 1980, 1981, 1982 e 1983

The model results, first present in time series, show a higher phytoplankton production in June, caused by the nutrients availability and increased sun radiation. After the bloom the phytoplankton concentration is controlled essentially by the zooplankton strong growth (not represented). Nitrate and ammonia are consumed during the phytoplankton

peak, afterwards ammonia increases due to zoo and phytoplankton respiration and excretion loses and nitrate increases due to nitrification processes.
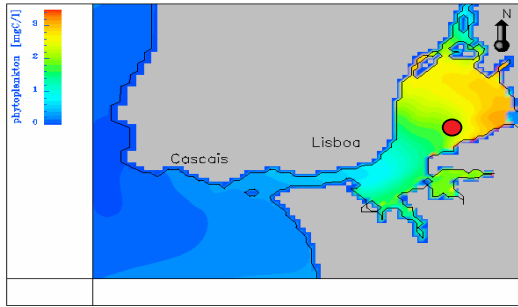
Figure 17 Field station 3.5 location
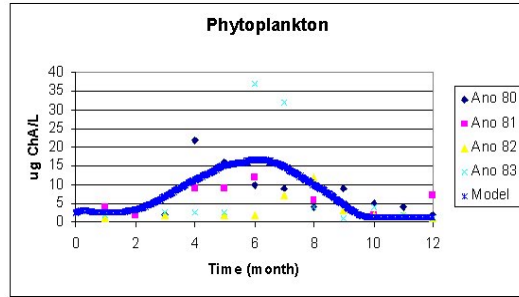
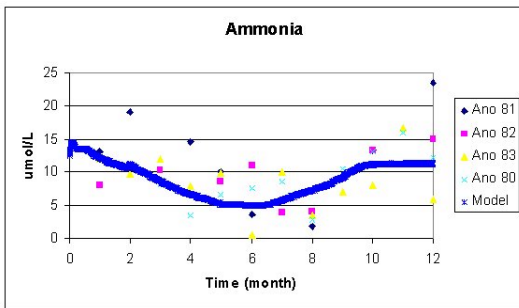Figure 18 - Phytoplankton variation over a year

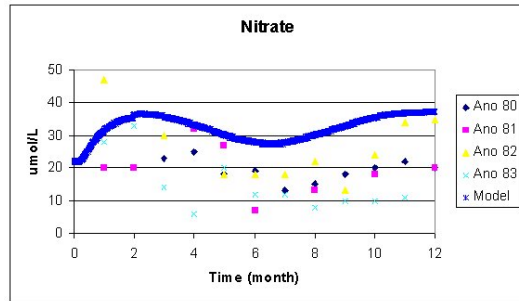Figure 19 - Ammonia variation over a year
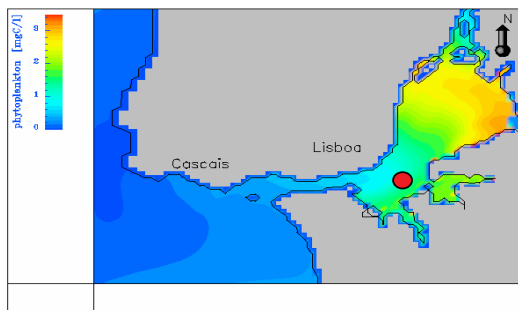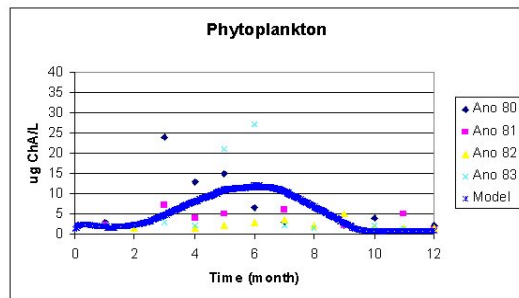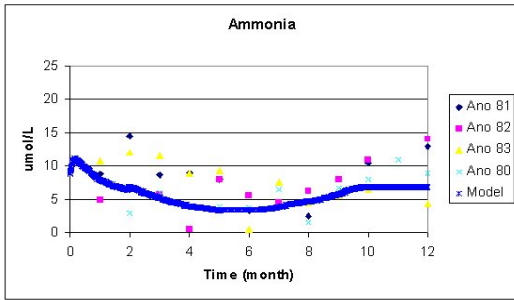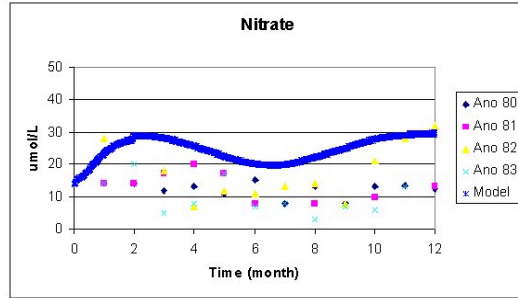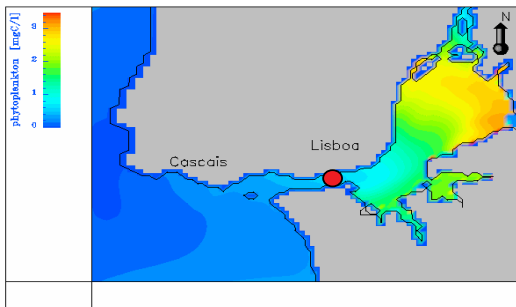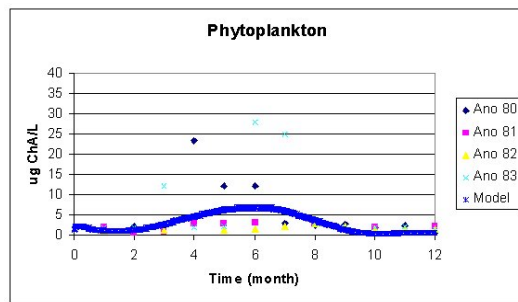

Figure 20 - Nitrate variation over a year

Figure 21 Field station 4.0 location
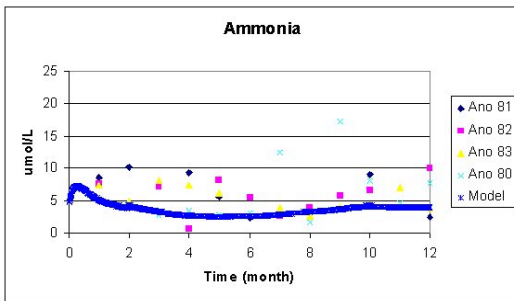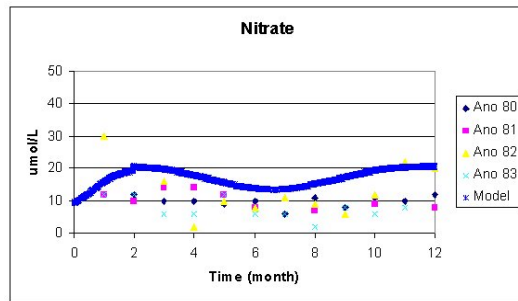

Figure 22 - Phytoplankton variation over a year

Figure 23 - Ammonia variation over a year

Figure 24 - Nitrate variation over a year

Figure 25 Field station 5.0 location

Figure 26 - Phytoplankton variation over a year

Figure 27 - Ammonia variation over a year

Figure 28 - Nitrate variation over a year

The next results show the spatial distribution of phytoplankton, nitrate and ammonia during the summer period (7, June 1999).
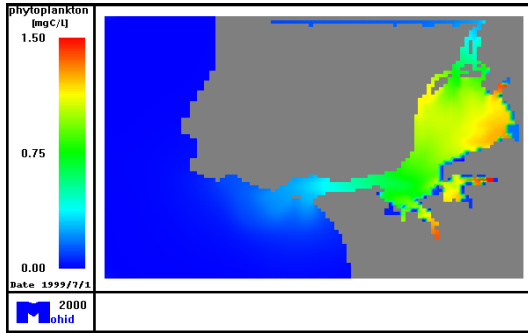
Figure 29 – Phytoplankton distribution at the Tagus Estuary.

Figure 29 shows high concentration of phytoplankton in the upper part of the estuary especially in the salt marsh region. Due to the low water level (more light available) and high nutrient concentration this region will have an intense production. The assimilation by phytoplankton preferably towards ammonia causes a strong depletion of nitrogen especially in the higher production areas (Figure 30 and Figure 31)
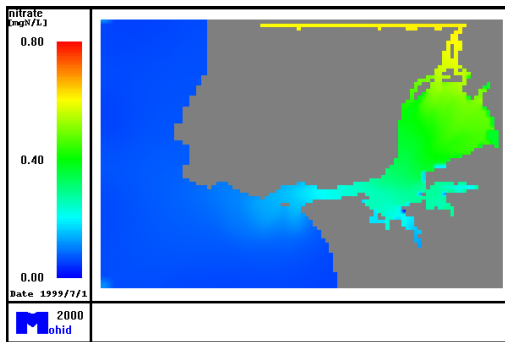

Figure 30 Nitrate distribution at the Tagus Estuary.
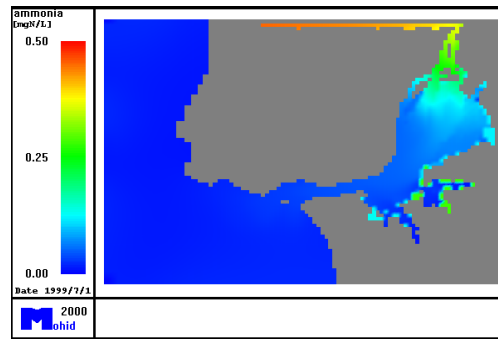
Figure 31 Ammonia distribution at the Tagus Estuary

The next pictures show the time and spatial integrated fluxes of phytoplankton, nitrate and ammonia over a year in the Tagus estuary.
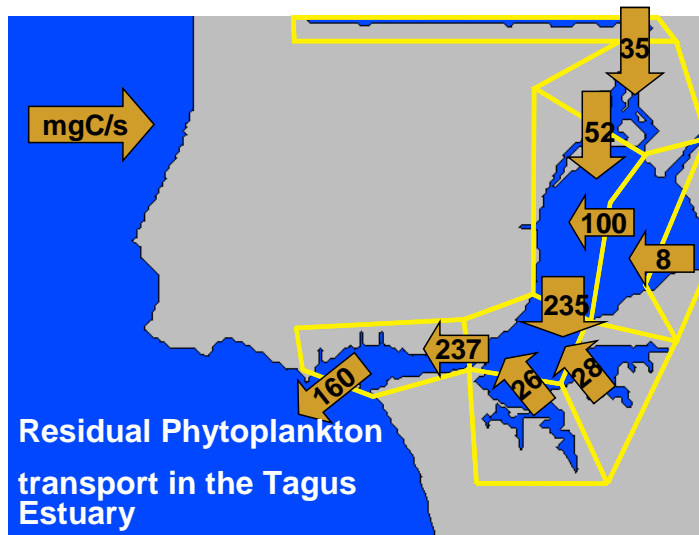
Figure 32 – Residual phytoplankton transport

In every case the estuary is exporting to the ocean. The phytoplankton fluxes (Figure 32) show that the river input it's very small so all the production occur inside the estuary and afterwards is exported to the ocean. The ammonia fluxes (Figure 33) show the estuary exporting less then it receives from river input. This can be explained by the fact of respiration and excretion loses being smaller then consumption by phytoplankton. With nitrate (Figure 34) the estuary exports to the ocean more then it receives from the river input. This mean that the source term of nitrate, nitrification, is higher then the sink terms, denitrification and assimilation by phytoplankton. This results are influenced by the fact that remineralization of organic nitrogen is accomplished in the water column because of the incapacity of the model to solve this process in the sediments. This fact gives an unrealistic mobility to remineralized nitrogen that could explain a higher output flux of nitrate.
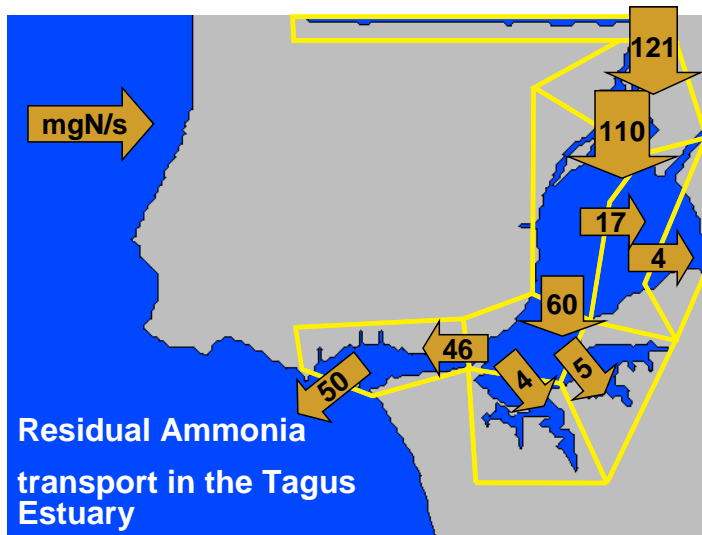
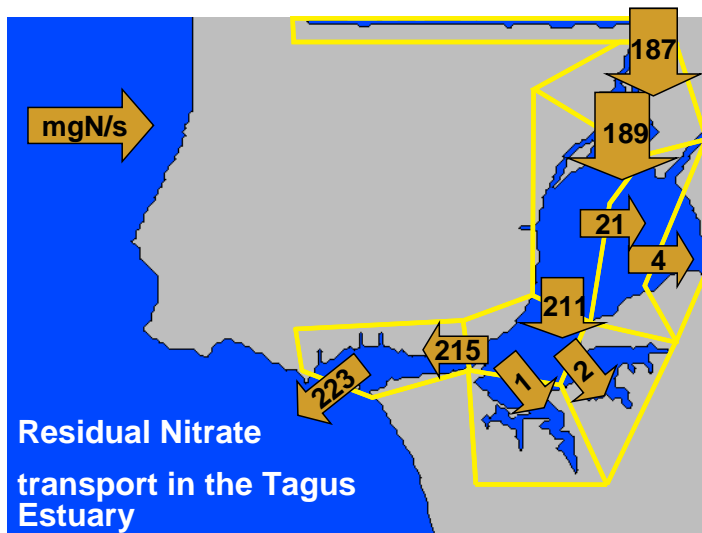Figure 33 – Residual ammonia transport.

Figure 34– Residual nitrate transport.

VI. References

Antunes, I. (2000) Modelação Matemática Da Qualidade Da Água No Estuário Do Tejo Dissertação para obtenção do grau de Mestre Instituto Superior Técnico, Universidade Técnica de Lisboa.

Arhonditsis, G., Tsirtsis, G., Angelidis, M.O., Karydis, M. (2000). Quantification of the effects of nonpoint nutrient sources to coastal marine eutrophication: application to a semi-enclosed gulf in the Mediterranean Sea. Ecological Modelling 129:. 209-227.

Baretta, J. W.; Ebenhöh,W.; Ruardji, P. (1995) The European Regional Seas Ecosystem Model, a complex marine ecosystem model. Netherlands Journal of Sea Research, 33: 233-246.

Brock, T. D. (1981) Calculating solar radiation for ecological studies. Ecological Modelling, 14:1-19.

Collins, C. D.(1980) Formulation and Validation of a Mathematical Model of Phytoplankton Growth. *Ecology*, **61**: 639-649.

Dronkers, J and J.T.F. Zimmerman, 1982. Some principals of mixing in tidal lagoons. Oceanologica Acta, 5: 107-117.

Eilers, P.H.C., Peeters, J.C.H. (1988) A model for the relationship between light intensity and the rate of photosynthesis in phytoplankton. Ecol. Modelling 42: 113-133.

EPA (1985) Rates, constants, and kinetics formulations in surface water quality modeling (2nd. ed.). United States Environmental Protection Agency, Report EPA/600/3-85/040.

Falkowski, P.G.; Wirick, C.D. (1981) A simulation model of the effects of vertical mixing on primary productivity. Mar Biol 65: 69-75.

Fasham, M. J. R.; Ducklow, H. W.; Mckelvie, S. M. (1990) A nitrogen-based model of plankton dynamics in the oceanic mixed layer. Journal of Marine Research, 48: 591-639.

Fransz, H.G.; Mommaerts, J.P. and Radach, G (1991). Ecological Modelling of the North Sea. Netherlands Journal of Sea Reserch 28 (1/2): 67-140.

Guillaud, J.-F.; Andrieux, F.; Menesguen, A. (2000). Biogeochemical modelling in the Bay of Seine (France): an improvement by introducing phosphorous in nutrient cycles. Journal of Marine Systems 25: 369- 386.

Humborg, C. ; Fennel, K., Pastuszak, M. Fennel, W. (2000). A box model approach for a long-term assessment of estuarine eutrophication, Szczecin Lagoon, southern Baltic. Journal of Marine Systems 25: 387- 403.

Jassby, A.D.; Platt, (1976) Mathematical formulation of the relationship between photosynthesis and light for phytoplankton. Limnol. Oceanogr 21: 540-547.

Kawamiya, M.; Kishi, M. J.; Suginohara, N.; (2000). An ecosystem model for the North Pacific embedded in a general circulation model Part I: Model description and characteristics of spatial distributions of biological variables. Journal of Marine Systems 24: 129- 157.

Kramer, K. J. M.; Brockmann, U. H.; Warwick, R. A.(1994) – Tidal estuaries: manual of sampling and analytical procedures. Published for the European Commission by A.BALKEMA/ROTTERDAM/BROOKFIELD, 304 pp.

Loureiro, J.M., 1979. Curvas de duração dos caudais médios diários no rio Tejo. DGRAH, Lisbon, p.1-18.

Martins, M. & Dufner, M.J.L., (1982). Estudo da qualidade da água. Resultados referentes às observações sinópticas em 1980. Estudo Ambiental do Estuário do Tejo (2ªsérie), nº 14. Comissão Nacional do Ambiente, Lisboa, pp.1-212.

Mehta, A. J. (1994). Hydraulic behaviour of fine sediment. Coastal Estuarial and Harbour Engineer´s Reference Book, E & FN SPON, Londres, 1984, c.39.

Mehta, A.J. (1986) Characterisation of cohesive sediment properties and transport processes in estuaries. In: Mehta AJ (ed.), Estuarine cohesive sediment dynamics. Springer, New York, p. 588 - 601

Mehta, A.J., (1988). Laboratory Studies on Cohesive Sediment Deposition and Erosion, Physical Processes in Estuaries, p 427-445, Springer-Verlag, Berlin, London

Miranda, R.(1996) The IST Water Quality Model- Technical Manual. DEM/IST. 30 pp.(*unpublished*).

Nakata, K.; Horiguchi, F.; Yamamuro M.(2000). Model study of Lakes Shinji and Nakaumi – a coupled coastal lagoon system. Journal of Marine Systems 26: 145- 169.

Napolitano, E. ; Oguz, T.; Malanotte-Rizzoli, P.; Yilmaz, A.; Sansone, E. (2000). Simulation of biological production in the Rhodes and Ionian basins of the eastern Mediterranean. Journal of Marine Systems 24: 277- 298.

Neumann, T. (2000). Towards a 3D-ecosysytem model of the Baltic Sea. Journal of Marine Systems, 25: 405-419.

Parsons, T. R., R. J. Lebrasseur, R. J. and J. D. Fulton (1967) – Some observations on the cell size and concentration of phytoplankton blooms. Journal of the Ocean. Soc. Of Japan, 23 (1):10-17.

Parsons, T.R.; Takahashi, M. & Hargrave, B. (1984) Biological oceanographic processes, 3rd. ed., Pergamon Press, Oxford, 330 pp.

Platt, T.; Galeggos, C.L.; Harrison, W.G. (1980) Photoinhibition of photosynthesis in natural assemblages of marine phytoplankton. J. Mar. Res. 38 :687-701.

Portela, L.(1996) Modelação matemática de processos hidrodinâmicos e de qualidade da água no Estuário do Tejo. Dissertação para obtenção do grau de Doutor em engenharia do Ambiente.Instituto Superior Técnico, Universidade Técnica de Lisboa. 240 pp.

Rivera, P.C. (1997) Hydrodynamics, sediment tranport and light extinction off Cape Bolinao, Philippines. PhD Dissertation. A.A.Balkema/Rotterdam/Brookfield.

Rodgers, P. and Salisbury, D. (1981) – Water quality modeling of Lake Michigan and consideration of the anomalous ice cover of 1976-77. *J. Great Lakes Res.* **7** (4): 467-480.

Somlyódy, L.; Koncsos, L. (1991). Influence of sediment resuspension on the light conditions and algal growth in lake Balaton. Ecological Modelling, 57: 173-192.

Steele, J. H. (1962) Environmental control of photosynthesis in the sea. Limnology and Oceanography, 7: 137-150.

Tetsuo Yanagi, Koh-ichi Inoue, Sigeru Montani, Machiko Yamada (1997) Ecological modelling as a tool for coastal zone management in Dokay Bay, Japan. Journal of Marine Sytems 13: 123-136.

Tett, P.; Wilson, H. (2000). From biogeochemical to ecological models of marine microplankton. Journal of Marine Systems, 25:431-446.

Thornton, K. W. and Lessen, A. S. (1978) A temperature algorithm for modifying biological rates. *Trans. Am. Fish. Soc.*, 107 (2): 284-287.

Vale, C., Sundby, B., (1987). Suspended sediment fluctuations in the Tagus estuary on semidiurnal and fortnightly time scales, Estuarine, Coastal and Shelf Science, 27: 495-508.

Valiela, I. (1995) Marine ecological processes. Springer-Verlag, New York. 686 pp.

van Rijn, L.C. (1989) Handbook – Sediment Transport by Currents and Waves. Report H 461 June. Delft Hydraulics.

Vanoni, V.A. (1975).   Sedimentation engineering, Report of Engineering Practice, Nº

54, Amer. Soc. of Civil Engineers, New York, 1975.

Vila, X.,Colomer, L.J., Garcia-Gil. (1996) Modelling spectral irradiance in freshwater in relation to phytoplankton and solar radiation. Ecological Modelling 87: 56-68.

Wollast, R. (1986). The Scheldt Estuary. In: W. Salomons, B.l. Bayne, E.K. Duursma and U. Förstner, Eds., Pollution of the North Sea. An assessment. Springer-Verlag, p. 183-193.

Krone, R.B. **,** **(**1962). Flume studies of the transport +in estuarine shoaling processes. Hydr. Eng. Lab., Univ. of Berkeley, California, USA.

Dyer, K.R. , (1986).   Coastal and estuarine sediment dynamics. Wiley-Interscience, New York.

Ross, M.A., (1988). Vertical structure of estuarine fine sediment suspensions, Ph. D. Dissertation, University of Florida, Gainesville, Florida.

Einstein, H.A., (1950).   The bedload function for sediment transportation in open channel flows. Soil Cons. Serv. U.S. Dept. Agric. Tech. Bull., Nº 1026, 78 pp.

Hayter, E.J. and Mehta, A.J., (1986)**.**   Modelling cohesive sediment transport in estuarine waters. Appl. Math. Modelling, 10: 294 - 303.

Partheniades, E., (1965)**.** Erosion and deposition of cohesive soils. J. Hydr. Div., ASCE, 91, No. HY1 : 105-139.

Mulder, H.P.J. and Udink, C., (1991)**.**   Modelling of cohesive sediment transport. A case study: The Western Scheldt Estuary. In: B.L. Edge, Ed., Proceed. 22nd Intern. Conf. Coast. Engin. Amer. Soc. Civ. Eng., New York, p. 3012 - 3023.

Stephens, J.A., Uncles, R.J., Barton, M.L. and Fitzpatrick, F., (1992)**.**   Bulk properties of intertidal sediments in a muddy macrotidal estuary. Mar. Geol. 103, 15pp.

Delo, E.A., (1988). Estuarine muds manual. Report Nº SR 164, Hydraulics Research, Wallingford, UK, 64 pp.

Winterwerp, J.C., Cornelisse, J.M., and Kuijper, C., (1991)**.** The Behaviour of Mud from the Western Scheldt Under Tidal Conditions. Delft Hydraulics, The Netherlands, Rep. z161-37/HW/paper1.wm, 14 pp.